THE ASTROPHYSICAL JOURNAL, 480:43–58, 1997 May 1
© 1997. The American Astronomical Society. All rights reserved. Printed in U.S.A.

GALAXY GROUPS, CDM/CHDM COSMOLOGIES, AND THE VALUE OF Ω_0

RICHARD NOLTHENIUS
University of California Observatories/Lick Observatory, University of California, Santa Cruz, CA 95064
ANATOLY A. KLYPIN
Department of Astronomy, New Mexico State University, Las Cruces, NM 88001
AND
JOEL R. PRIMACK
Physics Department, University of California, Santa Cruz, CA 95064
Received 1994 November 2; accepted 1996 October 11

ABSTRACT

We present techniques for identifying and analyzing galaxy groups and apply them to large-scale particle-mesh (PM) N-body simulations of structure formation in three $\Omega_0 = 1$ cosmological models: cold plus hot dark matter (CHDM), with $\Omega_{\rm cold} = 0.6$, $\Omega_\nu = 0.3$, and $\Omega_{\rm baryon} = 0.1$ at bias $b \equiv \sigma_8^{-1} = 1.5$; and two cold dark matter (CDM) models, at bias $b = 1.5$ and $b = 1.0$. Groups are identified with the adaptive friends-of-friends algorithm of Nolthenius. Our most important conclusions follow. The standard group M/L method gives $\Omega_0 \simeq 0.08$ for the CfA1 survey (for redshift link parameter $V_5 = 350$), and, applied to our $\Omega_0 = 1$ simulations, it gives $\Omega_0 \simeq 0.12$ for CHDM ($V_5 = 350$) and $\Omega_0 \simeq 0.35$ for CDM ($V_5 = 600$). This Ω bias appears to be even stronger at higher resolution. We show quantitatively how three different effects conspire to produce this large discrepancy, and we conclude that low observed Ω values need not argue for a low-Ω universe. Our preferred statistics of groups show promise in becoming powerful discriminators between Gaussian cosmological models, whose Ω_ν differ and are robust against several methods for assigning luminosity to dark matter halos, and for merging CfA1 data. However, our latest results at higher resolution show such strong sensitivity to how massive overmergers are broken up that more reliable ways of identifying luminous galaxies within large-scale simulations will be necessary before these statistics can provide reliable discrimination. When overmergers are broken up, the median virial-to-DM mass $M_{\rm vir}/M_{\rm DM}$ of three-dimensional–selected groups is ~ 1 for all simulations. Groups with $M_{\rm DM} > 10^{14}\ M_\odot$ appear virialized in all simulations. We measure global (not pairwise) velocity biases b_v, similar to previous studies. Within three-dimensional–selected groups, CHDM and CDM with $b = 1.5$ show a stronger bias of $b_v = 0.7$–0.8, while CDM with $b = 1.0$ shows groups of $b_v \simeq 1$.

Subject headings: cosmology: theory — dark matter — large-scale structure of universe — methods: numerical

1. INTRODUCTION

The simplest viable scenario of cosmic evolution begins with an $\Omega_0 = 1$ expansion seeded from inflation with Gaussian primordial fluctuations, with a Harrison-Zeldovich scale-invariant spectrum. These fluctuations later collapse via gravitational instability to form structure from galaxies on up. This picture has been remarkably resilient in the face of steadily mounting observations. The nature of the dark matter will govern how structure forms, and therefore may, in principle, be recoverable from the statistics of such structure (if not from direct detection as well). Evidence of structure on very large scales in the late 1980s began a series of efforts that have put severe constraints on standard cold dark matter (CDM; e.g., Baugh & Efstathiou 1993). This has motivated the investigation of alternative models with the desirable properties of significant power on large scales and low power on small scales, including cold + hot dark matter (CHDM). As recently emphasized by Pogosyan & Starobinsky (1995), if standard CDM fails, CHDM would remain the only theory compatible with the simplest and most aesthetic versions of inflation. Even more interesting, recent neutrino oscillation experiments provide preliminary (albeit controversial) evidence that at least one neutrino species indeed has a cosmologically important mass (Caldwell 1995; Primack et al. 1995).

Beginning with Klypin et al. (1993, hereafter KHPR), we explore in this series of papers the consequences of a universe dominated by cold + hot dark matter, and we compare it with standard cold dark matter and with observations. The CHDM model with $\Omega_\nu = 0.3$ has shown good agreement with observations of the galaxy correlation function and power spectrum (Baugh & Efstathiou 1993; Klypin, Nolthenius, & Primack 1997, hereafter KNP), the cluster-cluster correlation function (Holtzman & Primack 1993; Klypin & Rhee 1994), the variance and skewness of the Abell/ACO cluster distribution (Plionis et al. 1995; Borgani et al. 1997), the amplitude of the power spectrum from POTENT reconstruction of the local density field (Seljak & Bertschinger 1994; Kolatt & Dekel 1997), the *IRAS* Redshift Survey power spectrum (Fisher et al. 1993; Feldman, Kaiser, & Peacock 1994; KNP), quietness of the local Hubble flow (Schlegel et al. 1994), and the X-ray properties of clusters versus redshift (Bryan et al. 1994). However, recent work shows that CHDM with an Ω_ν as high as 0.3 conflicts with observations. Ghigna et al. (1994) analyzed the same simulations considered here and showed that CHDM with $\Omega_\nu = 0.3$ results in too many large voids, while Ghigna et al. (1996) show that a CHDM model with $\Omega_\nu = 0.2$ agrees well with the void probability function in redshift surveys. CHDM forms structure significantly later than most competing models, and recent observations of

damped Lyα systems (Storrie-Lombardi et al. 1995; assuming these can be associated with collapsed objects) are already showing a high enough number density at $z \sim 3$–4 to be in conflict with the $\Omega_\nu = 0.3$ used here (Klypin et al. 1995). There are also indications that fairly massive galaxies are apparently vigorously forming stars as far back as $z = 3$–3.5 (Steidel et al. 1996), and perhaps even $z \sim 4.5$ (Hu & McMahon 1996), which could rule out CHDM with $\Omega_\nu > 0.2$ (Mo & Fukugita 1996). Also, if preliminary evidence for clusters at high redshift (Giavalisco, Steidel, & Szalay 1994) is confirmed, Ω_ν's large enough to explain large-scale structure within the CHDM model may be ruled out. Here we will show that group analysis also tentatively points toward a lower Ω_ν. Finally, as for all $\Omega = 1$ models, the Hubble constant H_0 can be no larger than ~ 50 km s^{-1} Mpc^{-1} to stay within cosmic age constraints. Therefore, if the current observational evidence for $H_0 \simeq 70$–80 km s^{-1} Mpc^{-1} is confirmed, then CHDM at any Ω_ν, in its simplest and most aesthetic form, is ruled out. Throughout this paper, we assume $H_0 = 50$ km s^{-1} Mpc^{-1}.

We identify and analyze groups from the 100 Mpc 512^3 particle-mesh simulations described in KNP. The box size was chosen to give a good statistical sample of galaxy groups. With a mesh size of 195 kpc (perhaps typical of an $\sim L^*$ galaxy dark matter halo), we do not have the resolution to study individual galaxies. However, typical galaxy groups have virial radii of ~ 1–2 Mpc and begin to be resolved. The construction of the 512^3 grid of cells within the 100 Mpc box and the simulation calculation methods are described in KNP. Briefly, we use the "cloud-in-cell" approximation (Hockney & Eastwood 1981, eqs. [5]–[21]) for both the density assignment and force interpolation. The Poisson equation was solved using finite differences. A seven-point "crest" template was used to discretize the Laplacian operator, leading to Green's functions analogous to the two-dimensional case (Hockney & Eastwood 1981, eqs. [5]–[205]). The resulting system of linear equations was then solved by the fast Fourier transform technique.

In an earlier paper (Nolthenius, Klypin, & Primack 1994, hereafter NKP94), we showed how the statistics of galaxy groups can be used to discriminate between CDM and CHDM cosmologies and the CfA1 survey (Davis et al. 1982). In particular, rms group velocity $v_{\rm gr}$ (the rms velocity of all galaxies within the group, i.e., the conventional "velocity dispersion") versus the fraction of catalog galaxies in groups $f_{\rm gr}$ appeared to be a powerful discriminator. We deferred a more complete presentation to the present work. However, as we will see, group analysis statistics from new simulations of the "2-neutrino" (2ν) model (Primack et al. 1995) at higher resolution, using a breakup scheme based on a new, more evolved hydrodynamic CDM simulation from Evrard (1996, private communication) show strong sensitivity to the "overmerger problem" (Katz & White 1993). While we believe the $v_{\rm gr}$ versus $f_{\rm gr}$ statistics will eventually prove powerful discriminators, more reliable galaxy identification will be needed within large-scale cosmological models before group analysis can be confidently applied. Instead, we primarily focus here on group identification and calibration methods, and show how an $\Omega = 1$ universe can produce groups and clusters whose virial M/L naively imply $\Omega_0 \simeq 0.1$–0.2. This result appears quite robust. We also demonstrate how our group statistics could appear robust against the breakup of overmergers using the earlier available information, and yet show strong sensitivity with our later simulations. In the process, we also make a careful calibration of the grouping algorithm's Huchra-Geller–like velocity link criterion necessary to identify optimal groups in real surveys.

We analyze groups selected from two different versions of our catalogs. "Box groups" are identified from the complete 100 Mpc simulation boxes using full three-dimensional information. To make meaningful, direct comparisons with observations, we then make magnitude-limited "sky catalogs" in redshift space from each simulation, and then identify "sky groups" using criteria identical to those used on CfA1 data. The CfA1 catalog used here was extracted from the 1987 version of ZCAT.

Group analysis combines the information contained in both the velocity structure and the spatial structure of the galaxy distribution. Davé et al. (1997) presents complementary studies using these same simulations to devise statistics on the more purely spatial structure of the galaxy distribution. An accompanying computer visualization video sequence (Brodbeck et al. 1997, hereafter BHNPK) compares visually the differences between the simulations, sky catalogs, and the real universe. CDM structures are rather puffy filaments, with clusters at the intersections. By contrast, CHDM shows remarkably delicate filaments. Blurring in redshift space reduces the visual impression of these differences, yet their effect remains powerful on the statistics studied here.

Grouping in redshift space is done using the adaptive algorithm of Nolthenius (1993, hereafter N93). Tests with the original algorithm of Nolthenius & White (1987, hereafter NW87) gave essentially the same results but with slightly lower group velocity dispersions. Hierarchical methods (e.g., Tully 1987), on the other hand, produce a more severe ceiling on individual group velocity dispersions that would likely reduce our ability to discriminate between models. Recently, Frederic (1995a, 1995b) has claimed that the NW87 grouping algorithm velocity link seriously underestimates group velocity dispersions and therefore M/L ratios when compared with simulation groups. However, this study fails to emphasize the importance of the underlying cosmology to setting the grouping algorithm's appropriate link in redshift. Using only a low-bias $\Omega = 1$ standard CDM simulation, as Frederic did, will show that the NW87 redshift link normalization of $V_5 = 350$ km s^{-1} is too low (as already shown in NKP94) as a result of the less-concentrated structure and high-pairwise velocities in this model. The fault lies not in the algorithm, but in the assumption that this version of CDM is an appropriate calibrating cosmology for determining the merits for grouping algorithms used on real observations. One must first show that carefully analogous simulation data sets gives properties closely similar to those of the corresponding observations *over a broad range* of grouping linkages. Only then can the simulation be used to optimize grouping algorithm parameters. This is the approach taken here, as well as in NW87.

2. CONSTRUCTION OF THE GALAXY HALO CATALOGS

A detailed description of the simulation calculations is given in KNP and NKP94. Briefly, we use a particle mesh code on a a 512^3 grid, with 256^3 cold and 2×256^3 hot particles. The cold particle mass is 2.9×10^9 and 4.1×10^9 $M_\odot$ for CHDM and CDM, respectively. As before, we refer to the CDM $b = 1$ (somewhat lower than the latest 4 yr

COBE normalization; see Bennett et al. 1996) and $b = 1.5$ simulations as CDM1 and CDM1.5, respectively. The two CHDM simulations, CHDM1 and CHDM2, are both at $b = 1.5$ (consistent with the latest COBE normalization) and differ only in their initial conditions. The $CHDM_1$, CDM1 and CDM1.5 simulations all began with the same random number set describing the amplitudes of the initial waves perturbing the particles. The value of beginning each competing model with the same random perturbation set is that it guarantees that the same large-scale structures will emerge in each, so that differences between simulations will solely be the result of differences in the underlying physics of the evolution and not to cosmic variance. It was later found that this random number set had abnormally high power on large scales. The power spectrum was a factor of ~ 2 higher than typical on scales comparable to the box size. The probability of this occurring in any given realization was estimated at $\sim 10\%$ (KNP). As it turns out, there is good evidence that CfA1 has unusual large-scale power as well (see Baugh & Efstathiou 1993). A second CHDM simulation, $CHDM_2$, began with a much more typical spectrum.

A galaxy halo is defined as a mesh cell with a sufficiently high dark particle mass overdensity, $\delta\rho/\rho > (\delta\rho/\rho)_{\rm cut}$, at the end of the simulation ($z = 0$). We quantify the mass of a halo by the mass contained within a one-cell (or sometimes 3^3 cell) boundary. This is obviously crude. The boundaries are arbitrary, and no attempt is made (nor is it possible) to include only the gravitationally bound particles because of our limited spatial and force resolution.

When our purpose is to optimally delineate structure, we keep all cells above $(\delta\rho/\rho)_{\rm cut} = 30$, giving 29,151 halos in CHDM1; 37,164 in CDM1; 45,592 in CDM1.5; and 29,795 in $CHDM_2$. Constructing magnitude-limited redshift catalogs and attempting to match CfA1 galaxy number densities required higher, $(\delta\rho/\rho)_{\rm cut} = 80$–$150$, cutting galaxy totals by about 70%. Since each cell is 1/512 of the 100 Mpc box, or 195 kpc, a cell corresponds approximately to a dark matter halo surrounding a typical L^* galaxy.

3. BREAKING UP MASSIVE HALOS

One uncertainty in our earlier results is the possibility that the overmerging of dark matter galaxy halos may have significantly lowered the rms velocities of galaxies within groups, and perhaps also lowered the total fraction of galaxies in groups. Dark matter (DM) halos are extended, soft objects that merge easily. Galaxies undergo dissipative collapse to denser, smaller cross section objects that merge at perhaps only one-half the DM merger rate (Evrard, Summers, & Davis 1994, hereafter ESD). The dominant galaxy will tend to sit near the group center and have low center-of-mass velocity. By contrast, baryonic dissipation causes earlier collapse into several smaller but higher velocity galaxies (Katz & White 1993) whose merging rate is slower (ESD; Summers, Davis, & Evrard 1995). We now ask the following: above what halo mass $M_{\rm bu}$ does it become important? Katz & White (1993) find that some individual halos could be as massive as $1.5 \times 10^{14}\ M_\odot$. However, using reasonable M/L ratios, cooling efficiencies, and star formation rates, they argue most halos above $M_{\rm bu} = 5 \times 10^{13}\ M_\odot$ should be broken up, and that $M_{\rm bu}$ could be as low as $2.8 \times 10^{12}\ M_\odot$. Gelb (1992) finds too many halos above $V_{\rm circ} = (GM/r)^{1/2} = 350$ km s^{-1}, which, for r corresponding to our cell size, is equivalent to $3.4 \times 10^{12}\ M_\odot$. ESD also address this issue, and with better mass resolution they find a lower $M_{\rm bu}$ limit of $7 \times 10^{11}\ M_\odot$. Our most massive CHDM halo has 3^3 cell mass of $5 \times 10^{13}\ M_\odot$ (or a one-cell mass of $5 \times 10^{12}\ M_\odot$). To date, ESD remains the best-published work available on galaxy formation in groups and clusters in a dark matter background. Their Figure 12*a* provides a rough relation between dark matter halo mass and the number of galaxy-like objects ("globs" in their nomenclature) within the halo in standard CDM. They define the halo's mass as the mass within the sphere containing an average overdensity corresponding to virialization; $\delta\rho/\rho = 170$. Since ESD stopped at $z = 1$, we assumed collapsed, unevolving halo size from $z = 1$ to the present. The cosmological expansion factor of 2 then gives a corresponding $\delta\rho/\rho = 2^3 \times 170 = 1360$ for $M_{\rm bu}$ in our $z = 0$ simulations. We found the radius r_{1360} of this sphere by determining the radii of spheres encompassing the volume of our one-cell and three-cell masses, and assuming density fell linearly from the one-cell sphere radius to the three-cell sphere radius. The maximum radius allowed to enclose a single breakup candidate corresponded to the sphere enclosing a 2^3 cell volume, or halfway to the nearest allowable halo. This was done to avoid double counting some of the exterior mass. We then broke up halos whose mass $M_{1360} = M(r_{1360}) > 7 \times 10^{11}\ M_\odot$. The result of this procedure was $N_{\rm om} = 138$ ($CHDM_1$), 157 ($CHDM_2$), 571 (CDM1.5), and 658 (CDM1) halos identified as overmergers and suitable for breaking up into fragments. If mass is roughly proportional to light, observed galaxies suggest that fragments should be assigned Schechter-distributed masses. Dissipational hydrodynamic codes also produce gaseous galaxy-like objects with Schechter distributed masses (Evrard 1994, private communication; Frenk et al. 1996, hereafter FEWS). Therefore, we constrained the fragment masses to follow a Schechter distribution with the characteristic mass $M^* = \langle M/L \rangle L^* = 4.3 \times 10^{11}\ M_\odot$ (CHDM) or $1.08 \times 10^{12}\ M_\odot$ (CDM). L^* is $4.3 \times 10^{10}\ L_\odot$ from our CfA1 fit, and $\langle M/L \rangle$ is the median M/L of the simulation halos: 10 for CHDM, and 25 for CDM. The faint-end slope was set to the merged CfA1's $\alpha = -1.26$ (see § 6). Each overmerger was replaced with fragments of total mass M, where M was the virialized overdensity mass M_{1360} calculated above, minus the mass expected to be in fragments below the overdensity limit $(\delta\rho/\rho)_{\rm cut}$, selected for the simulation (and therefore too faint to see): 80 for both CHDM and 156 for both CDM simulations (see § 6). For all simulations, 16%–19% of the integrated Schechter function is contained in fragments below $(\delta\rho/\rho)_{\rm cut}$. For each overmerger, the brightest fragment was given a mass $M_{\rm bf} = (M_{\rm bu} M_{1360})^{1/2}$ (Evrard 1994, private communication) and placed at the original overmerger's position. Remaining masses were then randomly selected from a Schechter distribution, and each was randomly placed into any halo that could accept it without overfilling. This continued until a random fragment mass was generated that was too large to be added to any halo. At this point, all halos were $\sim 99\%$ full of fragments. Each set of fragments for a given halo was then ordered by mass and sequentially placed as close as possible to the parent halo cell while still enforcing the two-cell closest neighbor resolution limit. Thus, the most massive fragments were placed closest to the original DM center. Each fragment was then given a randomly oriented, random Gaussian velocity with dispersion equal to the rms velocity $V^{\rm om}_{\rm neigh}$ of all halos within 1 Mpc of the overmerged halo (or, in the few cases this did not include at least four

halos, out to the fourth nearest halo). The actual velocity distribution in such circumstances is poorly known, but simulations to date suggest Gaussian is approximately correct (Evrard 1995, private communication). The median values $\langle V^{\rm om}_{\rm neigh}\rangle_{\rm med}$ of these neighborhood rms velocities were ~ 300 km s^{-1} for all models, but individual overmergers ranged as high as ~ 1200 (CHDM) to ~ 2000 km s^{-1} (CDM1). Observations indicate that the brightest (assumed the most massive) galaxies in groups and poor clusters are moving at a center-of-mass velocity only ~ 0.25 that of their lower luminosity neighbors (Bird 1994). Therefore, we multiplied the brightest fragment's velocity by 0.25. The fragments of a given overmerger do not, at this point, satisfy the conservation of momentum. In the frame of the parent overmerger, the net momentum of the N fragments with masses m_i is $\sum_i^N m_i \boldsymbol{v}_i = \boldsymbol{p}$. To enforce momentum conservation, we correct each fragment velocity by adding a velocity differential $\delta \boldsymbol{v} = -\boldsymbol{p}(\sum_i^N m_i)^{-1}$. Finally, the masses were rescaled by $M_{1\ \rm cell}/M_{1360}$ so that they followed the one-cell convention used for all other cataloged halos. Three-cell masses were found in a similar way. The simulation halos we analyze below have all been subjected to this, our adopted breakup scheme. We also experimented with other breakup schemes. These are summarized in Table 1.

Our adopted scheme assigns to fragments their nearest neighbors' rms velocity $V^{\rm om}_{\rm neigh}$. An obvious alternative would be to use the circular velocity of the halo at virial overdensity radius, $V^{\rm om}_c = (GM_{1360}/r_{1360})^{1/2}$, where $\overline{\delta\rho/\rho}(r_{1360}) = 1360$. We decided against this for several reasons. First, the most appropriate mass and radius to use are unclear. Second, galaxies form early, and, in the dense environments common to these overmergers, it is the larger tidal field of the group that seems likely to eventually determine final fragment velocities. Finally, one of our goals was to evaluate how well the virial theorem measures mass in these systems, and enforcing dynamically determined velocities would bias these results. Figure 1 shows a scatter plot of $V^{\rm om}_c$ versus $V^{\rm om}_{\rm neigh}$ for each overmerger in the CHDM and CDM simulation boxes. The $V^{\rm om}_c$ and $V^{\rm om}_{\rm neigh}$ distributions differ substantially. However, their median values are very similar $\langle V^{\rm om}_c\rangle_{\rm med} \simeq \langle V^{\rm om}_{\rm neigh}\rangle_{\rm med}$, as shown in Table 2. Circular velocities are slightly higher than $V^{\rm om}_{\rm neigh}$; by $\sim 5\%$ for CHDM and by $\sim 15\%$ for CDM. Thus, using circular velocities would likely have raised our final group rms velocities by only a few percent, more so for CDM than for CHDM. On the other hand, virial velocities would have been lower than V_c. Note also that the extended tail of high $V^{\rm om}_{\rm neigh}$ is especially pronounced for the CDM models and is

TABLE 1

SUMMARY OF OVERMERGER BREAKUP METHODS

Method	Assumptions
Adopted	$M_{\rm bu} = 7 \times 10^{11}\ M_\odot$, M inside r_{1360} Schechter fragment masses M, $M^* = \langle M/L\rangle_{\rm sim} L^*_{\rm CfA}$, $\alpha = \alpha_{\rm CfA} = -1.26$ $\boldsymbol{v}_{\rm fragment}$ = Gaussian (σ, $\boldsymbol{v}_{\rm om}$),[a] σ = rms of galaxies within 1 Mpc or nearest 4 Fragments positioned by mass, higher mass closer to center Brightest fragment mass $M_{\rm bf} = (M_{\rm bu} M_{1360})^{1/2}$, at overmerger center, and velocity $\boldsymbol{v}_{bf} = 0.25 \times \boldsymbol{v}_{\rm fragment}$[a]
Method 1.....	$M_{\rm bu} = 7 \times 10^{11}\ M_\odot$, M inside r_{1360} Number fragments,[b] masses, if ordered, each is 90% of previous mass $\boldsymbol{v}_{\rm fragment}$ = Gaussian (σ, $\boldsymbol{v}_{\rm om}$),[a] σ = rms of 10 nearest galaxies Fragment positions not mass-dependent
Method 2.....	$M_{\rm bu} = 7 \times 10^{11}\ M_\odot$, M inside r_{1360} Schechter fragment masses M, $M^* = \langle M/L\rangle_{\rm sim} L^*_{\rm CfA}$, $\alpha = \alpha_{\rm ESD} = -1.35$ $\boldsymbol{v}_{\rm fragment}$ = random Gaussian (σ, $\boldsymbol{v}_{\rm om}$),[a] $\sigma = (GM_{1360}/r_{1360})^{1/2}$ Fragment positions not mass-dependent
Method 3.....	Leave simulation overmergers alone Merge CfA1 grouped galaxies within $r_{\rm proj} = 235$ kpc[c]

NOTE.—Fragment positions enforced two-cell limit, for all methods.

[a] Notation $\boldsymbol{v}_{\rm om}$ = velocity of original overmerger.

[b] From ESD Fig. 12*a*.

[c] NKP94 results.

TABLE 2

PROPERTIES OF BOX GROUPS

Simulation	$\rm CHDM_2$	$\rm CHDM_1$	CDM1.5	CDM1
Halo $(\delta\rho/\rho)_{\rm cut}$	80	80	156	156
$N_{\rm halo}$[a]	11305 (8585)	10898 (8134)	14636 (8503)	16050 (7247)
$N_{\rm om}$[b]	157	138	571	658
$V^{\rm om}_c$ km s^{-1}	309	316	315	322
$V^{\rm om}_{\rm neigh}$ km s^{-1}	283	319	266	291
$N_{\rm grps}$	641 (620)	576 (575)	727 (680)	619 (514)
$\langle M_{\rm vir}/M_{\rm DM}\rangle_{\rm med}$	1.26 (1.02)	1.43 (1.18)	1.27 (1.40)	1.44 (1.96)
$f_{\rm gr}$[c]	0.71 (0.70)	0.73 (0.71)	0.58 (0.50)	0.63 (0.52)
DM frac in groups[d]	0.15 (0.23)	0.14 (0.21)	0.23 (0.38)	0.27 (0.50)

NOTE.—Quantities in parentheses are for no-breakup case.

[a] Number of halos in the box.

[b] Number of overmerged halos.

[c] Fraction of halos which are in groups.

[d] Fraction of total DM which is inside the mean harmonic radius r_h of groups.

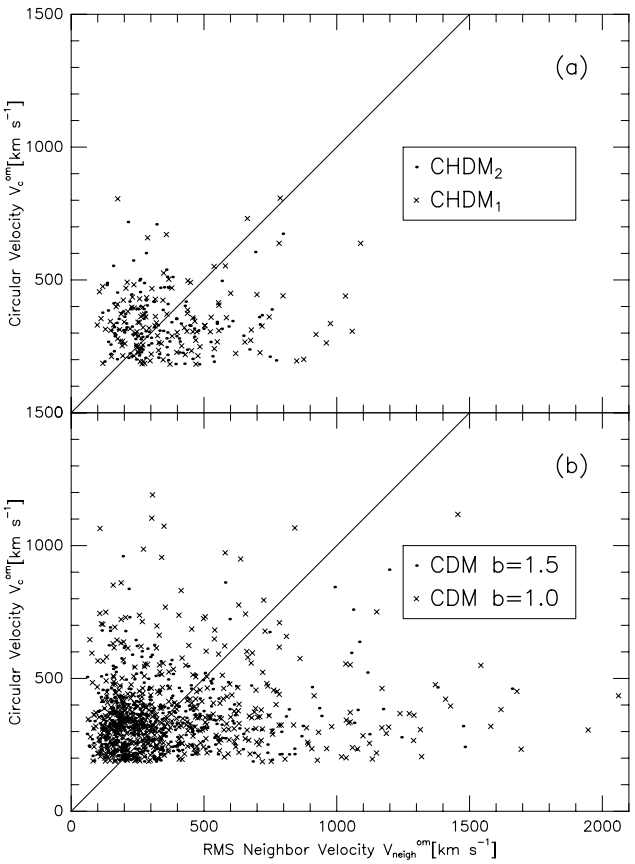

FIG. 1.—Comparison of the two methods of assigning velocities to the fragments of (*a*) CHDM and (*b*) CDM1 overmerger breakups. V_{neigh}^{om}, the rms velocity of all neighboring galaxies within 1 Mpc or within whatever larger radius encloses four neighbors, has a much wider range than the characteristic circular velocity $V_c^{om} = (GM_{1360}/r_{1360})^{1/2}$, yet the medians are very similar. CDM1 has a wider range for both velocities than does CHDM.

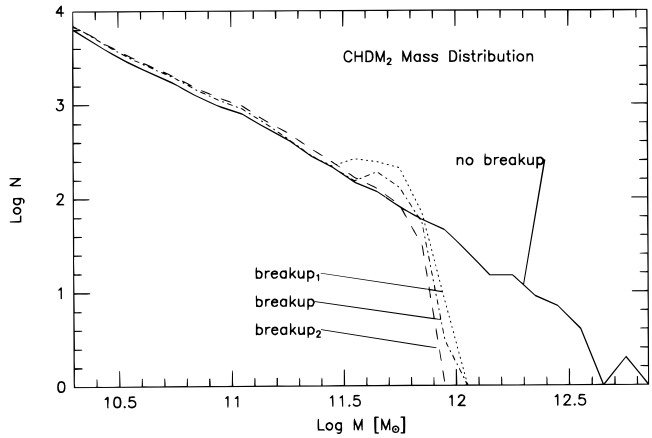

FIG. 2.—Comparison of the halo one-cell mass distribution for the different massive halo overmerger breakup methods. Our favored method is labeled "breakup," 'while methods 1 and 2 are labelled "breakup$_1$" and "breakup$_2$." The expression $d \log N/d \log M = -1.3$ below the breakup mass M_{bu}.

related to CDM, having higher pairwise and small-scale velocities than CHDM (KHPR; NKP94).

Another approach ("Method 3" in Table 1) is to leave the simulation halos alone and instead attempt to put real galaxies back into "overmerged" halos by merging them—i.e., taking a luminosity-weighted average of their positions and redshifts, then combining luminosities. In this case, one wants to merge CfA1 galaxies that are within about 1.5–2 cells ($\sim$350 kpc) on the sky, and within a velocity separation corresponding to the virial velocity of these massive halos, i.e., about 200–300 km s^{-1}. Since this is typical of the rms velocity of a medium-sized group. Method 3 turns out to correspond closely with the merging scheme already done in NKP94 (although the motivation then was actually to correct for spatial resolution, not overmerging).

Figure 2 shows the one-cell mass distribution of the halos. The no breakup halos follow a power law of slope $d \log N/d \log M = -1.33$. We stress that the one-cell and three-cell masses, being defined by arbitrary boundaries, are not particularly physical measures of dark matter halo mass, and in our analysis they are used only as stepping stones to luminosity. All of our breakup methods leads to a fairly sharp cutoff in masses at the upper end. Note that Method 1 makes an especially noticeable pile of fragment masses just below the breakup mass limit M_{bu}.

All of these breakup schemes may poorly estimate the number of fragments. Other purely dissipationless simulations (e.g., Carlberg 1994) find that dense DM cores are suprisingly persistent within virialized clusters, suggesting that overmerging may be less significant than generally believed. Also, if $M^*/10$ is equivalent to a luminosity of $L^*/10$, ESD and Evrard (1994, private communication) find too many fragments by an order of magnitude, when compared to observations. Our adopted procedure produces even more fragments (a median of eight fragments per overmerger for both CDM simulations and 14 for both CHDM simulations, with a maximum of $\sim$140 for all). On the other hand, Evrard's latest simulations, evolved to $z = 0$ and applied to our own higher resolution simulations, results in a much higher fraction of visible galaxies that are fragments (see § 9). Also, FEWS find that the number of baryonic "galaxies" within a DM halo is significantly higher when they turn dense baryonic globs of $M > 10^{10}\ M_\odot$ into stars at $z = 0.7$. Our luminosity assignment method (see § 6) produces a steep rise in M/L at low M (see Fig. 7) and prevents the overpopulation of visible fragments inferred in ESD, but perhaps may still not ensure the right fraction of visible galaxies which are the result of breakup. FEWS conclude that we do not yet have robust methods of simulating galaxy formation within DM halos, and we would agree.

4. PROPERTIES OF BOX GROUPS

We first describe groups selected using full three-dimensional spatial information from a complete sample of all galaxies above a rather low one-cell mass cutoff. The construction of the redshift space "sky catalogs" that can be compared to CfA1 data is described in § 6. A group is defined as the galaxies satisfying a specific group identification procedure designed to include all galaxies within a bounding surface of constant number overdensity. Our grouping scheme is the standard "friends-of-friends" algorithm. The critical link distance D is found from the N galaxies in the box above the mass cut by $D = D_0(l^3/N)^{1/3}$, where l is the length of the box and D_0 is the link parameter, expressed as the fraction of the mean interparticle spacing. For each galaxy, all neighbors within a distance D are linked. Each of the newly linked neighbors is in turn searched until no more members are found. We adopted $D_0 = 0.36$, corresponding to a minimum number overdensity for selected groups of $\sim$20, for three reasons: (1) in redshift

space, experiments show it produces a good compromise between selecting only the virialized cores of massive objects yet not merging separate groups by percolation (N93); (2) it produces a near maximum number of groups for statistical purposes; and (3) it facilitates comparison with earlier CfA1 group catalogs of N93 and Huchra & Geller (1982; hereafter HG82). This D_0 yields a fraction grouped of $\sim$70% for CHDM and $\sim$60% for CDM. In constructing groups near the box boundaries, the periodic images of galaxies were also considered during linking. This avoided the problem of clipping groups near the boundaries artificially.

Table 2 shows properties of groups made from the full box. The CHDM $(\delta\rho/\rho)_{\rm cut} = 80$ and CDM $(\delta\rho/\rho)_{\rm cut} = 156$ boxes, our fiducial boxes, turned out to best match CfA1 galaxy densities when halos were later assigned luminosities to make sky catalogs (see § 6). To facilitate comparison between CHDM and CDM at the same halo mass density cut, we also include $(\delta\rho/\rho)_{\rm cut} = 80$ CDM box results in Table 2. Note that these box groups are made from a volume-limited sample with a high fraction of low-mass galaxies and groups, unlike the later groups to be made from magnitude limited sky catalogs.

For our fiducial boxes, the mean spacing between groups is $\sim$9–12 Mpc for all simulations. However, groups are strongly concentrated along filaments surrounded by large voids (see BHNPK), so that the distance to the nearest neighboring group is generally smaller: 5 Mpc on average.

Figure 3 shows, for full boxes cut below $\delta\rho/\rho = 80$, the median group velocity dispersion $v_{\rm gr}$ versus the fraction of galaxies in groups $f_{\rm gr}$ as D_0 is varied. It is the real space analog of our favored statistic. All models show higher $v_{\rm gr}$ (i.e., "hotter") at low $f_{\rm gr}$, when only increasingly dense cores are selected. CHDM groups are much cooler than CDM groups, and CDM1 groups are significantly hotter than CDM1.5 groups.

Figure 4 shows the average distribution of mass around box groups in all simulations. Figure 4*a* also shows separate densities of the hot and cold fractions for $CHDM_2$. Since virial radii r_h ranged from $\sim$0.6 to $\sim$8 Mpc, we minimized smearing in distance by binning the mass about each group

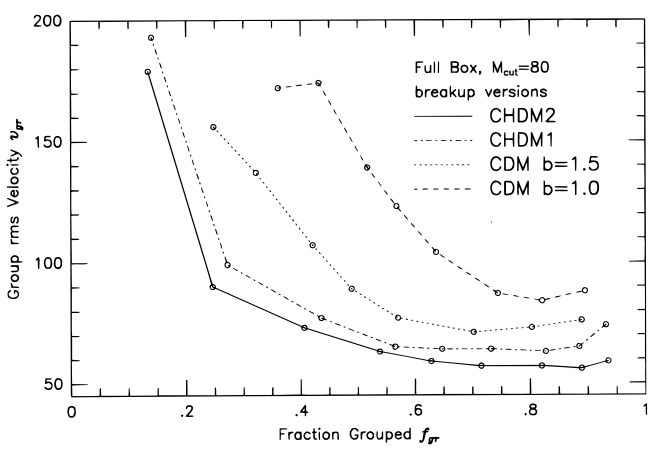

FIG. 3.—Median group rms velocity vs. fraction grouped for the full boxes cut at $\delta\rho/\rho = 80$. From the left-hand to the right-hand side, the points on each curve correspond to $D_0 = 0.10$, 0.15, 0.20, 0.25, 0.30, 0.36, 0.47, 0.58, 0.72. $D_0 = 0.10$ gave no groups for CDM1 and CDM1.5, and this point is skipped. At low $f_{\rm gr}$, only the dense cores of richer groups are selected, giving higher $v_{\rm gr}$ (but small sample size makes these points more uncertain).

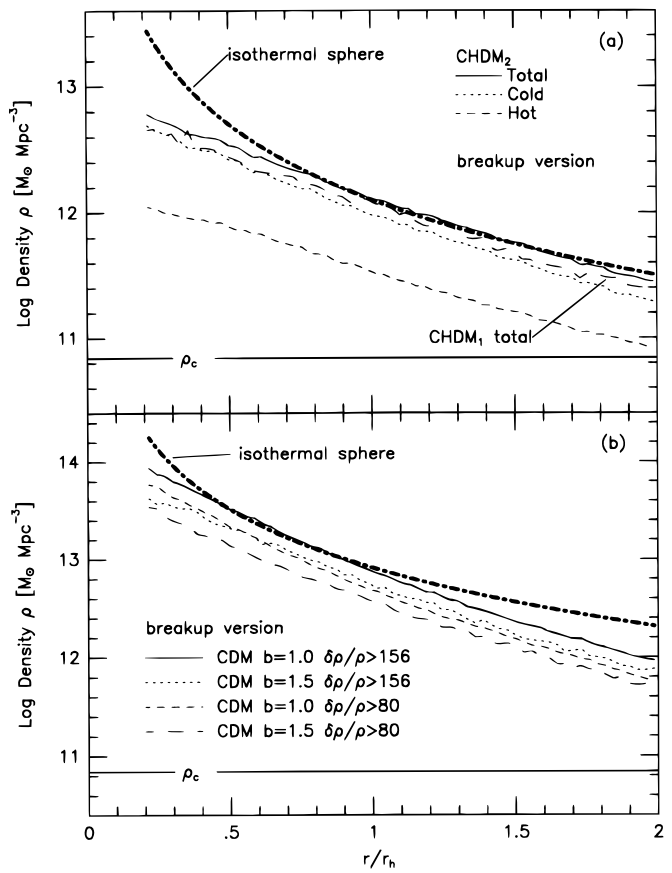

FIG. 4.—DM density distribution for (*a*) the CHDM box groups with halos of $\delta\rho/\rho > 80$, and (*b*) the CDM1 and CDM1.5 box groups with halos of $\delta\rho/\rho > 156$, compared to that for r^{-2} isothermal spheres. The origin $r = 0$ is the unweighted average of the position vectors of all member halos. Only the curve for total mass is shown for $CHDM_1$, while $CHDM_2$ shows the hot and cold distributions as well. Even at $r = 2r_h$, density is substantially above the critical density ρ_c. All simulations show an exponential $\rho(r)$, but CDM shows a steeper falloff than CHDM. Data inside $\sim$200 kpc is unresolved and not plotted.

as a function of the nondimensional radius r/r_h. The result is an unweighted average for all groups. The profile is approximately expoential $\rho \propto e^{-r/r_h}$. Beyond the core, a power law of slope of -2 (i.e., an isothermal sphere) fits the CHDM curves reasonably well. Simulations of galaxy clusters in a range of cosmologies (Crone, Evrard, & Richstone 1994) find that $\Omega = 1$ cosmologies show an isothermal DM distribution, while $\Omega_0 \simeq 0.2$ cosmologies do not. $CHDM_2$ densities are $\sim$10%–15% higher than $CHDM_1$. CDM densities, shown in Figure 4*b*, are also exponential. Groups made of halos over $(\delta\rho/\rho)_{\rm cut} = 156$ have densities on average $\sim$70% higher than those made of halos over $(\delta\rho/\rho)_{\rm cut} = 80$. The density distribution shows no detectable change of slope beyond the radius defined by the halos. Indeed, at $2r_h$ the density is still an order of magnitude above the critical density.

Figure 5 shows the cumulative mass for the fiducial boxes. Note that there is still a significant amount of mass from $r_h < r < 2r_h$ that appears to be part of the groups: $M(2r_h)$ is $2.7M(r_h)$ for CHDM and $2.0M(r_h)$ for CDM. Approximately 80% of the particles in this range have bound velocities. CDM box groups appear to contain a larger fraction of their DM mass at small r. Figure 5*b* shows the cumulative mass density distribution around sky groups. note that smearing in redshift space all but erases

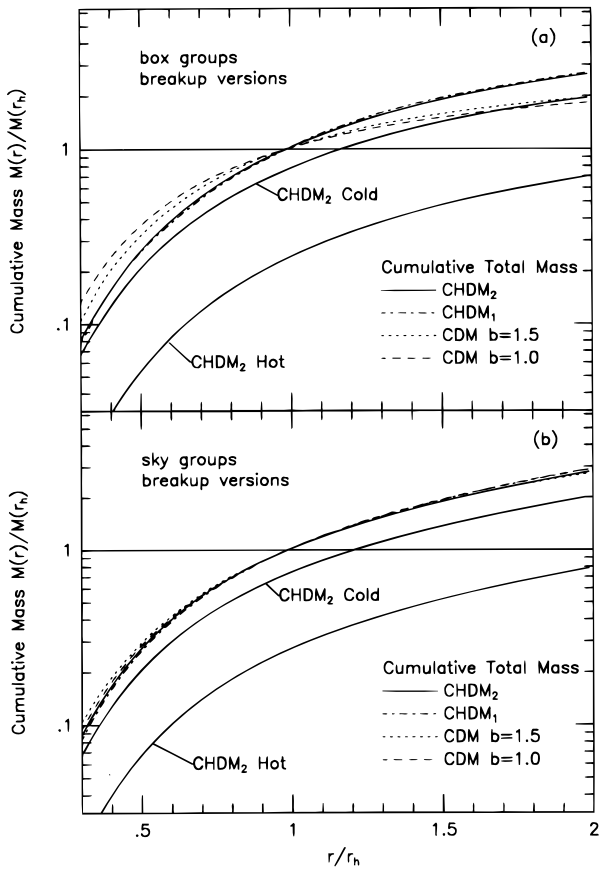

FIG. 5.—Cumulative mass distribution around (*a*) the fiducial box groups and (*b*) the fiducial sky groups. There is substantial mass outside but bound to the box groups; $M(2_r h)/M(r_h)$ is 2.7 for CHDM and nearly 2.0 for CDM. Around the sky groups, $M(2_r h)/M(r_h)$ is as high as 3.0 for all simulations. Blurring in redshift space reduces the differences between CHDM and CDM curves in the sky groups. Data inside $\sim$200 kpc is unresolved and not plotted.

the differences in the $M(r)$ trends between simulations. Sky groups are on average much brighter and more massive than box groups as a result of the magnitude limit. These more massive groups have an even broader distribution of surrounding dark matter, and $M(2r_h)/M(r_h)$ is 2.8–3.0 for all simulation groups.

In the cold + hot dark matter picture, the cold particles collapse into their gravitational potential wells first, later to be followed by the hot particles after they cool. This leads to a higher fraction of cold particles in the cores of the groups, shown in Figure 6. The $CHDM_1$ simulation's higher power on large scales seems to lead to a higher contrast between cold and hot densities, perhaps through earlier collapse and higher concentration of cold particles today. Data inside $\sim$200 kpc is unresolved and not plotted.

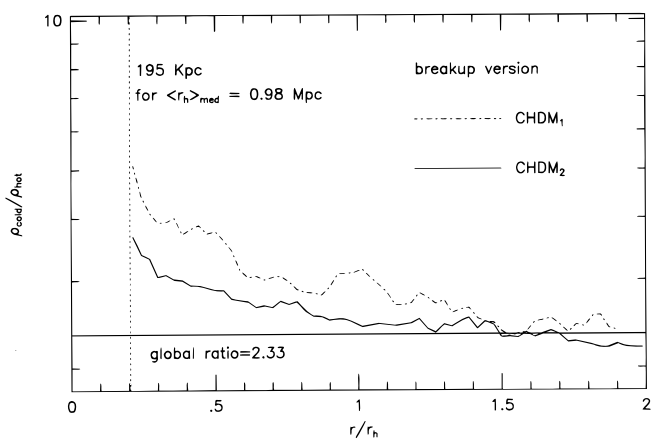

FIG. 6.—Ratio of cold to hot dark matter for the CHDM box groups (unweighted average over all groups). As for all boxes, small groups make up most of this volume-limited sample. Group cores are relatively dense and cold, with the hot particles predominately forming a more diffuse background.

5. MERGING THE CfA1 CATALOG

Several issues need to be considered before we can make realistic comparisons between simulations and CfA1 data. First, we must consider their differing spatial resolution. Galaxies are identified as cells at a local density maximum. Thus, the nearest possible neighboring halo will be two cells away. Therefore, we attempt to merge CfA1 galaxies that are sufficiently close. NKP94 used a simple merging sheme that assumed an isotropic orientation for the separation vector between all galaxies within a group and merged all galaxy pairs separated on the sky by less than $2r_{cl}/\pi$, where r_{cl} is the spacing between nearest possible neighbors averaged over the positions of all possible nearest neighbors, and $2/\pi$ projects this onto the sky. The isotropic assumption is actually incorrect. Isotropy would only be true if the depth of the group were as small as r_{cl}. Here we use an improved scheme described below.

For a given halo, the nearest possible neighboring halo will lie on a cube five cells on a side ("neighbor cube"), such that inside this cube the 26 immediately adjacent cells cannot be halos. Therefore, we average the lengths of the separation vectors between the parent halo and all cells on the neighbor cube, weighted by the frequency that the cell is actually occupied in the simulations, yielding a closest neighbor three-dimensional distance of $r_{cl} = 0.509$ Mpc. We seek to merge CfA1 galaxies closer than $r_{cl}/2$ (those between $r_{cl}/2$ and r_{cl} are balanced, on average, by those between r_{cl} and $1.5r_{cl}$). Since candidate mergers will have sky-projected separations of order $r_{proj} \leq 0.25$ Mpc, while a typical group's depth is of order 1.5–2 Mpc, most pairs close on the sky should not be merged and the isotropic estimate of NKP94 results in too many CfA1 mergings. To model the probabilities properly, we constructed suites of artificial groups with realistic dimensions and density distributions, and calculated the probabilities that two-dimensional close pairs were three-dimensional close pairs and should be merged. Applying these probabilities to CfA1 close pairs in several trials gave a final catalog in which 39 group members and five binaries were merged. Note that this is only 2% of the sample.

6. CONSTRUCTING SKY-PROJECTED REDSHIFT CATALOGS

All current large-scale simulations suffer from our poor understanding of how to assign luminosities to masses in order to compare with real observations. For our one-cell masses, we have therefore made the simple assumption that the baryonic mass in each $(195 \text{ kpc})^3$ cell turns into stars in such a way that the resulting luminosity function $\phi(L)$ has a Schechter form similar to that of the merged CfA1 catalog, and that galaxy luminosity increases monotonically with one-cell mass. While a monotonic $L(M)$ is plausible, we note

that the simulations of Navarro, Frenk, & White (1996) suggest that bright galaxies of a range of $v_{\rm circ}$ inhabit halos of surprisingly similar mass.

We assume a luminosity function of Schechter (1976) form, and the parameters α and M^* for the merged CfA1 catalog were determined using a code based on the inhomogeneity-independent method of de Lapparent, Geller, & Huchra (1989, hereafter DGH), assuming simple, unperturbed Hubble flow distances $D = V/H_0$ (except that radial velocities $V < 300$ km s^{-1} are set to $V = 300$ km s^{-1}). ϕ^* was constrained by requiring that the appropriate integral N over the solid angle A inside $V = 12{,}000$ km s^{-1} produce the observed number of galaxies N in the CfA1 catalog,

$$N = \frac{A\phi^*}{H_0^3} \int_{300}^{12000} v^2 \Gamma[\alpha + 1, \lambda(V)] dv \qquad (1)$$

and

$$\lambda(V) = \frac{L_{\rm lim}(V)}{L^*} = {\rm dex}\left[0.4\left(M^* - 14.5 + 25 + 5 \log\left(\frac{V}{H_0}\right)\right)\right], \qquad (2)$$

where $L_{\rm lim}(V)$ is the luminosity of an $m = 14.5$ galaxy at redshift V, and V/H_0 is in Mpc. Our ϕ^* constraint differs from the maximum-likelihood methods (e.g., Efstathiou, Ellis, & Peterson 1988) or that of DGH, yet it reproduces their unmerged CfA1 ϕ^*'s well.

To generate the sky catalogs, we first made fiducial groups from the full box using three-dimensional information. The $\sim$8–10 most massive clusters ("Virgo's") in the CHDM$_1$ box were centered about, and within a factor of 2–3 of, the adopted Virgo mass of $M_{\rm virgo} = 2.5 \times 10^{14}\ M_\odot$. Corresponding CHDM$_2$ clusters were less massive. We placed an observer on a "home galaxy" 20 Mpc away from one of these clusters. We then chose luminosity assignment parameters $(\delta\rho/\rho)_{\rm cut}$, the lowest halo mass retained, and Schechter parameters α and M^*, and generated N Schechter distributed magnitudes to be paired with the N halos above $(\delta\rho/\rho)_{\rm cut}$ in such a way that the luminosity as a function of halo mass $L(M)$ rose monotonically. We then observed the box, keeping galaxies above apparent magnitude $m = 14.5$ out to $V = 12{,}000$ km s^{-1}. Radial velocities v_r in direction $\boldsymbol{r}$ at distance r were calculated from

$$v_r = (\boldsymbol{v} - \boldsymbol{v}_0) \cdot \boldsymbol{r} + H_0 r\ , \qquad (3)$$

where the observer's home galaxy has peculiar velocity $\boldsymbol{v}_0$. Because of redshift distortion, the observed α is $\sim$0.4 steeper and the observed M^* is $\sim$0.4 brighter than the input values for our simulations, requiring us to iterate until we fit the observed CfA1 α, M^*, and projected galaxy density. These $L(M)$ parameters were then used to do a random search in the CHDM$_1$ and CHDM$_2$ boxes for candidate home galaxies that satisfied the following conditions: (1) the local galaxy density in redshift space ($V < 750$ km s^{-1}) was within a factor of 1.5 of that in the merged CfA1 galaxy density (though still unusually on the low side), and (2) the closest Virgo-sized cluster was 20 Mpc away in distance. Among these candidates we chose six that were distributed as widely through the box as possible. Since the CDM1 and CDM1.5 boxes had the same initial random wave amplitudes as CHDM$_1$, the locations of large clusters and filaments were essentially the same as for CHDM$_1$. In order to further remove noise caused by cosmic variance when comparing the different cosmological models, we therefore chose the six viewing locations within CDM1 and CDM1.5 to be on the halos nearest to the viewing halo coordinates found for CHDM$_1$. The resulting home galaxies had an average peculiar velocity of $V_{\rm pec} \simeq 800$ km s^{-1}. A final iteration then adjusted our $L(M)$ parameters slightly so that the Schechter functions of the six sky catalogs matched that of the CfA1.

Since we retained all data out to $V = 12{,}000$ km s^{-1} and our 100 Mpc box corresponds to only 5000 km s^{-1} for $H_0 = 50$ km s^{-1} Mpc^{-1}, this required replicating periodically each simulation box on all of its faces. However, at greater distances, only the brightest galaxies are retained in our magnitude-limited catalogs, so the replica boxes are sampled sparsely. The effect of replication simply means we are taking medians from a smaller sample of unique groups than would otherwise be the case for a volume of this size, and should be unimportant.

To approximately simulate boundary effects but still retain a large sample of the sky, we excised a 20° wide "zone of avoidance," leaving a solid angle of $A = 10.384$ sr. We also generated a second set of sky catalogs that had the local "virgo cluster" rotated to its CfA1 position, and the CfA1 latitude and declination limits imposed, giving a solid angle of $A = 2.66$ sr. All results turn out to be quite insensitive to these boundary and sample size differences. Because of periodic boundary conditions, each galaxy appears $\sim$3–4 times in the $A = 10.384$ sr catalogs, and $\sim$1.8 times in the $A = 2.66$ sr catalogs. To see whether our statistics were sensitive to the cluster positioning, we experimented using viewing locations on roughly L^* halos without regard to cluster locations, and found that $f_{\rm gr}$ dropped by $\sim$1%–3% and $v_{\rm gr}$ remained essentially unchanged.

We found that setting the apparent magnitude $m = 14.5$ for a halo of $(\delta\rho/\rho)_{\rm cut} = 80$ (CHDM) and 156 (CHDM) at $V = 300$ km s^{-1} (therefore retaining all CfA1 data) produced a total density of halos $\sim$0%–20% above that of the merged CfA1 catalog. The difference between $(\delta\rho/\rho)_{\rm cut} = 80$ and 156 has only a minor effect on the sky catalogs, since the imposition of an apparent magnitude limit means that only a few percent of sky catalog galaxies have $\delta\rho/\rho < 156$. (By contrast the volume-limited box sample is dominated by low-mass halos and groups because of the steep mass function.) Random culling down to CfA1 density then yielded our final sky catalogs. The 10.384 sr catalogs each had 9204 galaxies inside a redshift of 12,000 km s^{-1}. All 2.66 sr catalogs had 2358 galaxies within 12,000 km s^{-1}.

Our adopted breakup procedure produced a relatively high fraction of fragments in the sky catalogs: 27% (CHDM), 50% (CDM1.5), and 61% (CDM). Using breakup Method 1, a high percentage of sky catalog galaxies were also fragments of overmergers: 27% for CHDM and 70% for CDM. These percentages were only 11% (CHDM), 37% (CDM1.5), and 46% (CDM) for Method 2, which had many more low-mass fragments.

Figure 7*a* shows M/L for all of our sky catalogs. While M/L diverges upward at the smallest masses (which comprise only a tiny fraction of the sky catalog members), for the great majority of galaxies $M/L \sim 10$ for CHDM and $M/L \sim 20$–25 for CDM. Figures 7*b* and 7*c* show the distribution of one-cell masses in the sky catalogs. Note that breaking up the overmergers produces a strong peak for the

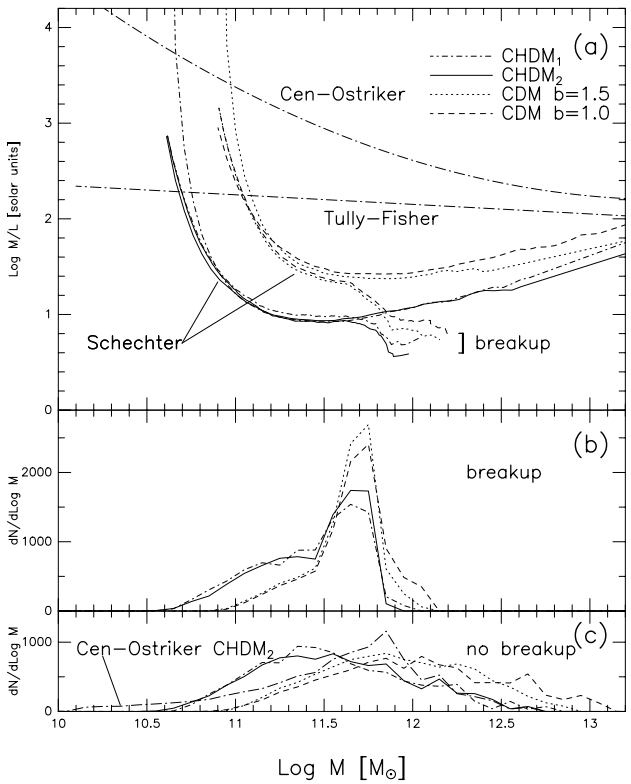

FIG. 7.—(*a*) Assigned one-cell mass-to-light ratio required in order to reproduce the CfA1 Schechter luminosity function parameters, for each simulation. The high M/L for low-mass halos and breakup fragments keeps most of them out of the sky catalogs. Also shown is M/L for the Cen-Ostriker and Tully-Fisher prescriptions, which place much higher L on faint, nearby, low-mass galaxies, and for which no attempt is made to agree with observations. (*b*) The distribution of no breakup sky catalog galaxies vs. mass. (*c*) Breaking up overmergers clips the high end and makes a large number of fragments below $M_{\rm bu}$.

fragments, just below the cutoff mass $M_{\rm bu} = 7 \times 10^{11}\ M_\odot$. This is especially true for CDM, which has higher mass halos than CHDM.

Our resulting sky catalogs had Schechter parameters $\alpha \sim -1.22$ and $M^* \sim -21.21$, compared to CfA1's $\alpha \sim -1.27$, $M^* = -21.09$ for both merged and unmerged versions. The average peculiar velocity for the home galaxies was $852 \pm 99{,}595 \pm 247{,}700 \pm 127$, and 991 ± 169 for the sky catalogs of $CHDM_1$, $CHDM_2$, CDM1.5 and CDM1, respectively, where the $\pm 1\ \sigma$ range is over the six sky catalogs of each model.

To examine the sensitivity of our comparisons to luminosity assignment, we considered two alternative methods. Cen & Ostriker's (1993, hereafter CO93) hydrodynamic simulations imply a relation between CDM total density contrast $\hat{\rho}_{\rm tot}$ (dark matter + gas/stars) and collapsed baryonic density contrast $\hat{\rho}_{\rm baryon}$ (presumably stars), where, in general, $\hat{\rho} \equiv \rho/\bar{\rho}$ and $\bar{\rho}$ is averaged over an appropriate smoothing length R: $\log(\hat{\rho}_{\rm baryon}) = A + B \log(\hat{\rho}_{\rm tot}) + C \log^2(\hat{\rho}_{\rm tot})$. Extrapolating CO93's trends down to $R = 0.6$ Mpc (for three-cell masses) then gave $B = 2.3$, $C = -0.20$. Normalizing catalogs to CfA1 density gave $A = 6.23$ (CHDM) and $A = 5.8$ (CDM). the resulting luminosity functions were Schechter-like, but with M^* 2.5 mag too bright (~ -23.5) and α too steep (~ -1.7). The resulting halo M/L (see Fig. 7*a*) attaches much higher L's to massive galaxies, relative to the Schechter prescription, favoring distant, luminous galaxies at the expense of those nearby.

The second alternative method uses the blue Tully-Fisher relation of Fouque et al. (1990), which defines the absolute B magnitude M_B of the galaxy as $M_B = -5.5 \log(V_{\rm circ}) - \beta$, where β is a calibration and we set $V^2_{\rm circ} = GM_{\rm cell}/r_{\rm cell}$. This is equivalent to $M^{1.1}/L = \text{const}$. Our adopted β's, selected to match the merged CfA1's 866 $\rm sr^{-1}$ galaxy density, are significantly lower than Fouque et al.'s since our halos are much larger and less concentrated than observed disks. Applied to our halos, the resulting relation attaches much higher L's to low-mass halos, relative to the Schechter prescription. This leads to catalogs with an unrealistic proportion of nearby galaxies and therefore heavily weights fainter, lower $v_{\rm gr}$ groups.

7. TUNING THE GROUPING ALGORITHM LINK PARAMETERS

Conventionally, a group is thought of as a collapsed, gravitationally bound collection of perhaps three to 50 galaxies. For our purposes, we consider a group more generally as any set of galaxies that satisfy linking criteria on the sky and in redshift. Any viable cosmological model must be able to produce a set of such groups whose typical properties are in good agreement with identically selected real groups *for any link lengths.* It is not necessary that the groups be bound, let alone collapsed or virialized. Nevertheless, it is also of interest to identify that set of groups that is closest to satisfying the conventional definition. While minimizing contamination by interlopers is important, e.g., for estimating Ω_0 from the M/L method (see § 8), it is even more important that the collective group properties most closely match those for groups of comparable overdensity identified using full three-dimensional information. The corresponding link criteria that make these most realistic groups are referred to below as the "fiducial" links.

We use the adaptive grouping algorithm of N93, which is a modification of the original friends-of-friends algorithm in redshift space given by HG82. Galaxies at redshift V km $\rm s^{-1}$ are linked if the separation on the sky is less than $D_L(V)$ and their difference in redshift is less than $V_L(V)$, where

$$R^{\rm sky}_{\rm M.I.S.}(V) = \frac{2}{\pi}\,\phi^*\Gamma[1+\alpha,\,\lambda(V)]\,, \tag{4}$$

$$D_L(V) = D_n\,R^{\rm sky}_{\rm M.I.S.}(V_0)\left[\frac{\Phi(V_0)}{\Phi(V)}\right]^{1/2}\left(\frac{V_0}{V}\right)^{1/3}, \tag{5}$$

$$V_L(V) = V_5\left[\frac{\Phi(5000\ \text{km s}^{-1})}{\Phi(V)}\right]^{1/3}. \tag{6}$$

Equation (3) gives $\lambda(V)$. V_0 is an arbitrary redshift distance used for scaling, here taken to be 1000 km $\rm s^{-1}$. D_n, an input parameter, is the sky link expressed as a fraction of the sky-projected mean interparticle spacing $R^{\rm sky}_{\rm M.I.S.}$. The expression $\Phi(V)$ is the integrated galaxy luminosity function above the apparent magnitude limit visible at redshift V. $D_L(V)$ is designed to ensure that a group at the minimum number density contrast just meets the selection criteria at all redshifts V (see NW87). We scale V_L with the mean interparticle spacing. We chose this scaling, rather than the linear NW87 scaling [whose resulting groups $(M/L)(V)$ trend actually turned out to match slightly better to groups selected using full three-dimensional information at the same overdensity limit], simply because it produced a flatter distribution of group M/L with distance. We have also run cases with the

TABLE 3

V_5 LINK BEST MATCHING THREE-DIMENSIONAL GROUPS' v_{gr}'s[a]

Simulation	$CHDM_2$	$CHDM_1$	CDM1.5	CDM1
V_5	368 (375)	397 (348)	571 (485)	669 (576)
$\langle v_{gr}\rangle_{med}$	121 (119)	123 (119)	183 (162)	225 (202)

[a] V_5 link giving redshift space groups with the same $\langle v_{gr}\rangle_{med}$ as three-dimensional groups, at fiducial $D_n = 0.36$. All in km s^{-1}, no breakup case is in parentheses.

NW87 version of the $V(L)$ algorithm, and find negligible differences in group properties and no change in our conclusions. For the purposes of comparing models, either $V_L(V)$ can be used. We parameterize the size of the link in redshift with $V_5 \equiv V_L(5000 \text{ km s}^{-1})$.

Our goal is to identify groups in redshift space that most nearly match their corresponding true overdensities in real space, and our most relevant property to match is the velocity dispersion of the group. Therefore, we identify the V_5 required to produce the same median v_{gr} as is seen in groups selected using full three-dimensional information on our fully corrected simulations at the same fiducial $D_n = 0.36$ (see Table 3). This is $V_5 \simeq 350$–400 km s^{-1} for CHDM, $V_5 \simeq 550$ km s^{-1} for CDM1.5, and 670 km s^{-1} for CDM1. If no breakup is performed, v_{gr}'s are very similar, but generally require slightly lower V_5's to match up with three-dimensional groups.

As confirmation, we note that the fraction of galaxies grouped f_{gr} will at first rise steeply with V_5 as new members are rapidly added from the dense region containing the group. The f_{gr} (V_5) curve will then show a distinct drop in slope as it enters the interloper regime, when essentially all valid members have been added, and primarily outliers and interlopers from the lower density surroundings are incorporated at higher V_5. Figure 8 shows that this transition occurs near $V_5 \sim 350$ km s^{-1} for both CHDM simulations and near $V_5 \sim 600$ km s^{-1} for both CDM simulations, similar to the v_{gr} criterion above. Therefore, we adopt $V_5 = 350$ km s^{-1} as the fiducial redshift link for CHDM and $V_5 = 600$ km s^{-1} as that for CDM. Note that, unlike the v_{gr} criterion, this measure can also be applied to real data, and it yields an optimal $V_5 = 350$ km s^{-1} for the CfA1 curve on Figure 8.

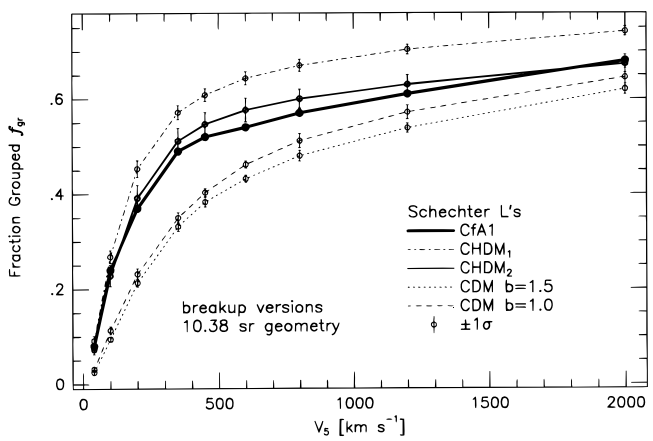

FIG. 8.—Fraction of galaxies in groups f_{gr} vs. V_5 for all simulation sky catalogs. On this and later sky catalog curves, error bars are $\pm 1\,\sigma$ over the six viewpoints. The curves flatten when primarily the nonmember outliers in low-density regions begin to be incorporated into groups at V_5 too high.

8. THE DYNAMICAL STATE OF THE GROUPS AND IMPLIED Ω_0

To assess the dynamical state of groups, we calculated the number-weighted virial mass estimator for three-dimensional–selected box groups. This is the M_{vir} appropriate if the mass is dominated by a dark matter background distributed like the galaxies, and it is given by

$$M_{vir} = \frac{2\sigma r_h}{G}, \tag{7}$$

where, for a group of n galaxies, $\sigma = (n-1)^{-1}\sum_i (\boldsymbol{v}_i - \langle \boldsymbol{v}\rangle)^2$ is the three-dimensional rms velocity about the mean velocity $\langle \boldsymbol{v}\rangle$ of the group. We then compared this to the true mass M_{DM} in dark particles within the mean harmonic radius r_h, where

$$r_h = \frac{n(n-1)}{2\sum_{i<j}^{n} r_{ij}^{-1}}, \tag{8}$$

and r_{ij} is the separation between galaxies i and j.

Figures 9*a* and 9*b* show scatter plots of group log M_{vir} versus log M_{DM} for the no breakup and breakup CDM boxes, respectively. Many of the smaller no breakup CDM

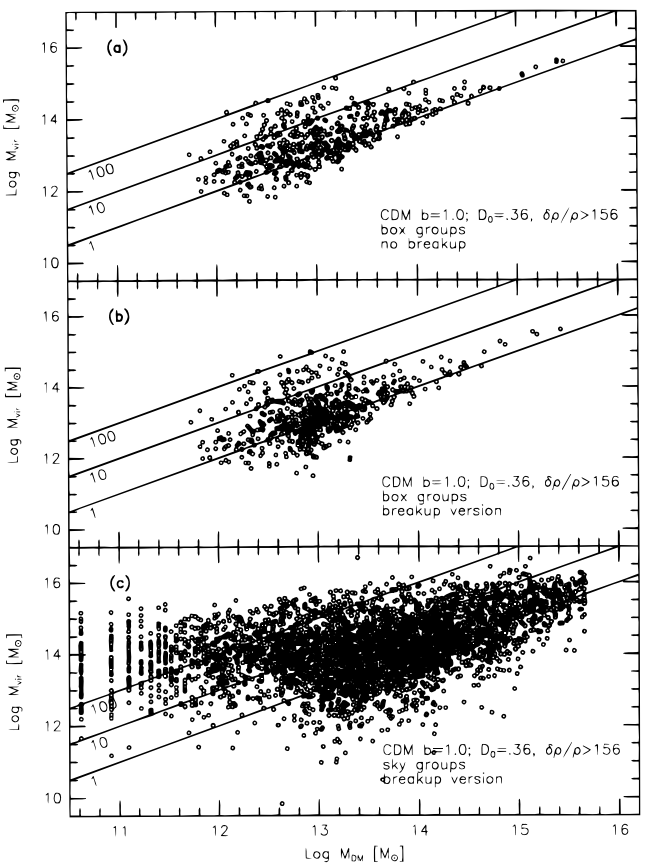

FIG. 9.—Number-weighted virial mass estimator M_{vir} from the halos vs. the dark matter M_{DM} contained within the mean harmonic radius r_h defined by the halos, for three-dimensional selected box groups in CDM1. The no breakup case (*a*) has a significant tail of high M_{vir}/M_{DM} groups, while the breakup case (*b*) includes many more $M_{vir}/M_{DM} \sim 1$ groups. Higher pairwise velocities in CDM cause the extended tail to high M_{vir}/M_{DM} in both cases. The combined sky groups for all six viewpoints (*c*) show a strong bias toward high M_{vir}/M_{DM} at low mass, as high small-scale velocities mean that small sky groups are not bound.

groups appear to be unbound, with the median $M_{\rm vir}/M_{\rm DM}$ biased as high as 2.0 for CDM1. Breaking up the overmergers reduces this bias significantly. This effect is not caused by the higher minimum halo overdensity [$(\delta\rho/\rho)_{\rm cut} = 156$ vs. $(\delta\rho/\rho)_{\rm cut} = 80$ for CHDM], since it is also clearly seen in the $(\delta\rho/\rho)_{\rm cut} = 80$ CDM boxes. It also appears equally strong when only better sampled groups (at least 10 members) are considered. The explanation is that many small groups do not appear in the no breakup cases because of overmerging. Recall that a halo is defined as a local density maximum, requiring neighboring cells to be relatively underdense. Also, a group must contain at least three members to be identified. The overmerged CDM halos often dominate their surroundings to such an extent that too few other local density maxima can be defined, preventing a group from being identified. When these are broken up, new groups result. These groups turn out to have $M_{\rm vir}$ close to $M_{\rm DM}$, on average, so that their inclusion lowers the median $M_{\rm vir}/M_{\rm DM}$ nearer to unity. This issue affects CDM much more than CHDM, since CDM has ~ 4 times as many overmergers (see Table 2).

Note that the breakup case in Figure 9*b* still has these high $M_{\rm vir}/M_{\rm DM}$ groups. Correlating high $M_{\rm vir}/M_{\rm DM}$ in the no breakup CDM box with other group properties, we found that these groups tend to be poorly sampled (all groups with $M_{\rm vir}/M_{\rm DM} > 30$ have 5 or fewer members), have higher than average size, low-density contrasts, high-peculiar velocities, and tend to lie in denser regions. Using computer visualization and color-coding groups by their $M_{\rm vir}/M_{\rm DM}$ shows that these groups tend to be small, as well as lie near the outer parts of dense clumps and filaments. All this suggests that these groups may have experienced tidal shearing sufficient to unbind them. Other recent work supports this idea (e.g., Mamon 1994). Some high $M_{\rm vir}/M_{\rm DM}$'s are no doubt simply a result of the inherent high noise in $M_{\rm vir}$. Figure 9*c* shows $M_{\rm vir}$ versus $M_{\rm DM}$ for groups from all six fiducial linked 10.38 sr catalogs. Note that the high V_5 required to match median three-dimensional $v_{\rm gr}$'s nevertheless produces a tail of spurious groups with high $v_{\rm gr}$, little mass within r_h, and therefore high $M_{\rm vir}/M_{\rm DM}$. The high V_5 link essentially produces a floor for $M_{\rm vir}$, which is unreasonably high for the smallest groups. This is a general feature of all group catalogs linked in redshift space (see Geller & Huchra 1983, hereafter HG32; Ramella, Geller, & Huchra 1989, hereafter RGH). Banding in these plots is the result of using only a 10% sample of the dark particles; the smallest (spurious) groups contain only a few dark particles.

The corresponding plots for the CHDM boxes are in Figure 10. CHDM box groups appear little changed by breakup, partly because they contain only one-fourth as many overmergers, and partly because they show lower random velocities on small scales. Note in Figure 10*c* that the lower V_5 level appropriate for CHDM significantly reduces the problem of spurious high $M_{\rm vir}/M_{\rm DM}$ groups. If, as the present study suggests, a low V_5 is also appropriate to the real universe, the problem of contamination and spurious groups may not be as severe as seen in, e.g., Geller & Huchra (1983).

Massive groups ($M > 10^{14}\ M_\odot$) in all boxes appear to define a narrow $M_{\rm vir}/M_{\rm DM}$ that appears clearly virialized, yet that lies systematically higher than the virialization line. There are two biases toward high $M_{\rm vir}/M_{\rm DM}$, which likely account for this, and which are present for all groups. First, the r_h sphere within which particles are counted is centered

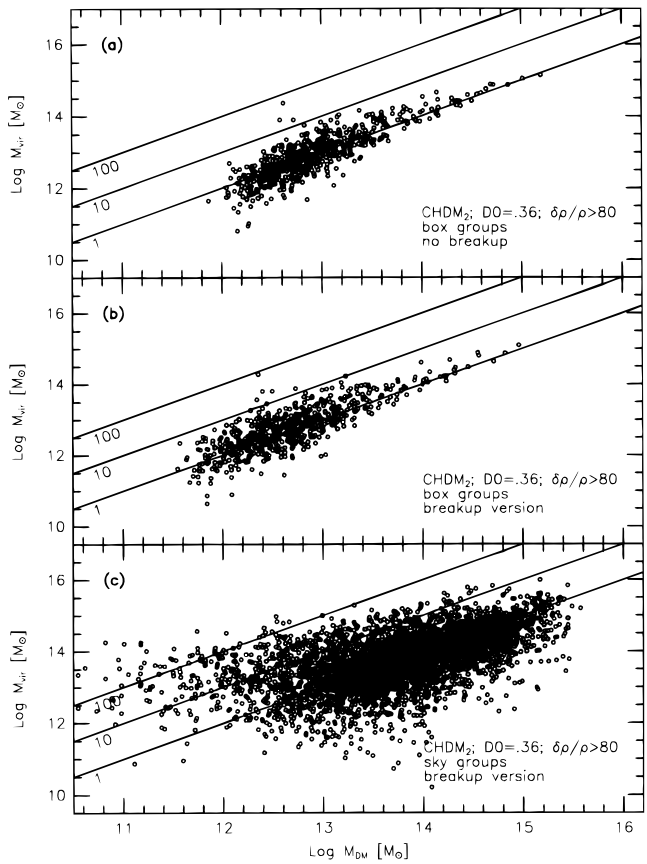

FIG. 10.—Same as Fig. 9, but for CHDM$_2$. There is little difference between the (*a*) no breakup and (*b*) breakup cases, and the low pairwise velocities make for less bias and less noise in the (*c*) sky groups' $M_{\rm vir}$ than seen in CDM.

on the mean position of the halos. Centering instead on the dark particle concentrations lowers $M_{\rm vir}/M_{\rm DM}$. We confirmed this by centering on the mass-weighted mean position of the particle condensations within $1.5r_h$ of the groups, and found it raises $M_{\rm DM}$ such that median $M_{\rm vir}/M_{\rm DM}$ is lowered by 7%. Second, many groups, especially the larger ones, are elongated density enhancements along filaments. Counting within a sphere will include spurious low density areas along the "equator" while missing the high-density regions along the "poles." If this bias is $\sim 30\%$ in $M_{\rm DM}$, which seems plausible (see group geometries in the video sequence of BHNPK), then $M > 10^{14}\ M_\odot$ groups in the breakup boxes appear to obey the virial theorem, on average, in all simulations.

We also determined several measures of the "velocity bias" b_v (Carlberg & Couchman 1989)—the velocity of the galaxies compared to that of the underlying cold dark matter particles. In KNP, we considered pairwise velocities. Here we are interested in the virial properties, and the relevant velocity biases are defined differently. The global velocity bias $b_v^{\rm global}$ is defined by a sum over the i galaxies and j DM particles within the box $b_v^{\rm global} = (\sum_i v_{i\rm gal}^2/\sum_j v_{j\rm DM}^2)^{1/2}$. The results are summarized in Table 4, using all halos with one-cell mass above $1.5 \times 10^{10}\ M_\odot$. The velocity bias within a group's r_h is defined over the i galaxies and j DM particles as $b_v^{\rm grp} = [\sum_i (\boldsymbol{v}_i - \langle \boldsymbol{v}_{\rm gal}\rangle)^2/\sum_j (\boldsymbol{v}_j - \langle \boldsymbol{v}_{\rm DM}\rangle)^2]^{1/2}$, where $\langle \boldsymbol{v}_{\rm gal}\rangle$ is the mean unweighted galaxy velocity and $\langle \boldsymbol{v}_{\rm DM}\rangle$ is the mean DM particle velocity within the group. Figure 11 shows that $b_v^{\rm grp}$ is fairly noisy for low

TABLE 4

VELOCITY BIAS

Simulation	$b_v^{\rm global}$	$\langle b_v^{\rm grp}\rangle_{\rm avg}$	$\langle b_v^{\rm grp}\rangle_{\rm med}$
$CHDM_1$.....	0.94 0.90)	0.85 (0.78)	0.78 (0.76)
$CHDM_2$.....	0.93 (0.89)	0.76 (0.69)	0.73 (0.71)
CDM1.5.....	0.83 (0.79)	0.82 (0.74)	0.78 (0.79)
CDM1.....	0.96 (0.90)	1.08 (0.92)	1.00 (1.06)

NOTE.—the no breakup case is in parentheses.

and moderate mass groups (and more so for CDM), but is confined quite closely about the global median for the virialized log $M_{\rm DM} > 13.8$ clusters. CHDM galaxies show a moderate bias but only within groups. CDM1.5 is moderately biased both globally and inside groups. CDM1 galaxies, however, show essentially no bias in or out of groups, in agreement with $b_v^{\rm global} = 0.94$ *from* Katz, Hernquist, & Weinberg's (1992) hydrodynamic simulation.

The standard method for estimating Ω_0 from bound virialized groups is to assume all galaxies have, on average, the same mass-to-light ratio M/L, given by the median M/L for groups, then integrating over the luminosity function to get the mass density (Kirschner, Oemler, & Schechter 1979). For a Schechter luminosity function this means

$$\Omega_0 = \frac{8\pi G}{3H_0^2}\left\langle\frac{M}{L}\right\rangle\phi^*L^*\Gamma(\alpha+2)\,. \tag{9}$$

Table 5 shows the resulting inferred Ω_0 using the fiducial grouping algorithm parameters and Schechter $L(M)$ for the sky catalogs. Means and standard deviations are over the six viewpoints. Using the Cen-Ostriker $L(M)$ gives very similar Ω's. No $N(z)$ corrections (see § 9) were applied to get $\langle M/L\rangle_{\rm med}$, since group M/L is virtually independent of redshift.

All of our $\Omega = 1$ simulations yield low observed Ω's. Thus, these simulations show a feature that has been seen in real data for over a decade and that has been used by some to argue for a low-Ω universe: How can Ω be 1 if bound groups and clusters consistently account for only $\simeq$10%–20% of the mass? Three factors can explain this discrepancy.

1. Only the mass within the mean harmonic radius r_h of the groups is measured by the virial estimator. We see in Figure 4 that density falls approximately like an isothermal sphere outside group cores, and that this continues to at least $2r_h$ (about midway to the next nearest group, on average), where the cumulative mass $M(2r_h) = 3M(r_h)$ (see Fig. 5b). This additional factor of 3 in mass is almost certainly bound to the groups, since $\rho(2r_h) \simeq 4\rho_c$(CHDM) to $10\rho_c$(CDM), infall is still occurring, and a check shows that over 80% of the particles between r_h and $2r_h$ have gravitationally bound velocities. The fraction of the total mass in the box that lies within the r_h sphere of fiducial linked groups is only $\sim$15%–25%, as shown in Table 6. Most mass lies outside of groups. As stated earlier, however, most of the halos (60%–70%) are inside groups.

2. The relevant virial velocities appropriate for measuring the local mass are actually those of the individual particles, not the galaxies. As seen in Table 4 and Figure 11, the median velocity bias within CHDM groups is $\sim$0.75. Since $M_{\rm true}/M_{\rm vir} \propto 1/b_v^2$, this contributes another factor of 1.8 to the estimate.

3. We have also assumed spherical symmetry in Figures 4 and 5. The true shape of groups is more elongated, as structure is still quite stringy at this point in the evolution. The inappropriately counted matter along the "equator" of the

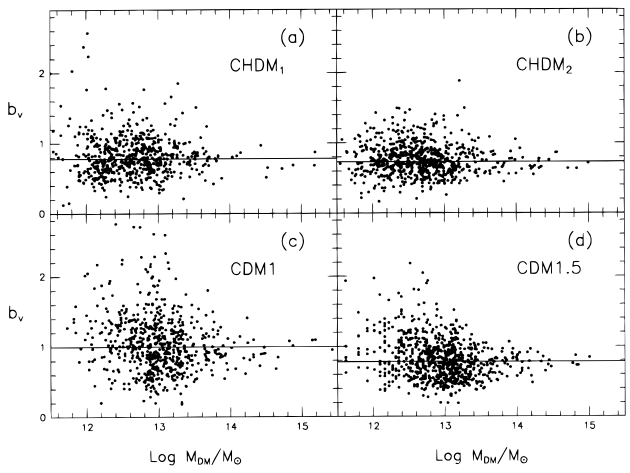

FIG. 11.—Velocity bias parameter b_v for all box groups at the fiducial link. The horizontal lines define the median values. $CHDM_2$ has a significant bias of $b_v = 0.7$. CDM1 shows almost no net velocity bias. $CHDM_2$'s low pairwise velocities lead to a tighter distribution. The banding in CDM1.5 (*d*) is a result of the small subsample of dark particles used in the calculations.

TABLE 5

Ω_0 FROM GROUP M/L METHOD

Catalog	V_5	avg $\langle M/L\rangle_{\rm med}$	Ω_0
CfA1 (full)[a]	350	62	0.06
CfA1 (merged).....	350	79	0.08
$CHDM_1$	350	128 ± 18 (150 ± 11)	0.13 ± 0.02 (0.14 ± 0.01)
$CHDM_2$	350	134 ± 18 (126 ± 13)	0.12 ± 0.02 (0.11 ± 0.01)
CDM1.5	350	158 ± 21 (178 ± 12)	0.17 ± 0.02 (0.18 ± 0.02)
CDM1	350	171 ± 27 (183 ± 44)	0.18 ± 0.02 (0.19 ± 0.04)
CfA1 (full)[a]	600	119	0.12
CfA1 (merged).....	600	152	0.15
$CHDM_1$	600	188 ± 25 (207 ± 21)	0.19 ± 0.02 (0.19 ± 0.01)
$CHDM_2$	600	212 ± 30 (193 ± 21)	0.20 ± 0.03 (0.17 ± 0.02)
CDM1.5	600	322 ± 35 (347 ± 32)	0.34 ± 0.03 (0.34 ± 0.04)
CDM1	600	343 ± 63 (395 ± 34)	0.36 ± 0.06 (0.40 ± 0.03)

NOTE.—No-breakup results in parentheses.

[a] Full, unmerged CfA1 catalog.

TABLE 6

MASS, VOLUME FRACTION WITHIN BOX GROUPS

Simulation	N_{grps} [a]	f_{mass} [b]	f_{volume} [c]
$CHDM_1$.....	575	0.14	0.0086
$CHDM_2$.....	640	0.15	0.0072
CDM1.5.....	736	0.23	0.0038
CDM1.....	617	0.27	0.0026

[a] Number of groups in box.
[b] Fraction of box mass which is within r_h of groups.
[c] Fraction of box volume which is within r_h of groups.

groups is of lower density and fails to compensate for the uncounted high-density regions missing above the "poles" by perhaps a factor of ~ 1.3. The product of these factors (~ 7) approaches an order of magnitude.

While item 1 is closely related to the fact that the galaxies are a biased ($b = 1.5$) tracer of the DM, it seems likely that the less clustered hot DM, especially that filling the voids (see BHNPK), will additionally bias M/L to the low side. Together, these factors show that, within the assumptions of this method, an observed $\Omega_0 \simeq 0.1$ can indeed be consistent with a true $\Omega = 1$ universe. In fact, real clusters are already showing that out to just beyond the optical radius, gravitational lensing finds masses roughly a factor of ~ 2 higher than virial estimates (e.g., Fahlman et al. 1994). FEWS also find that their high-resolution hydrodynamical simulations of a rich cluster give a similarly severe underestimate of the true Ω. There are other problems with the M/L method. For example, the stellar populations of groups and especially clusters is well known to be older and have lower M/L than is typical for the field.

Our Ω at $V_5 = 350$ for the CHDM simulations is 50% higher than that for the merged CfA1 at the same V_5. $\Omega_{CHDM} = 0.12$ versus $\Omega_{CfA1} = 0.08$, due almost entirely to the difference in the groups' mean harmonic radii, which enters in the virial estimator. Our Ω for the full CfA1 is smaller than that of HG82's $\Omega_0 \simeq 0.1$ (for the nearby, all-sky $m < 13.2$ CfA sample, and smaller than RGH's $\Omega_0 \simeq 0.13$. As we have argued here and elsewhere (NW87, N93), we prefer a significantly smaller redshift link than that used by these authors, which directly lowers the velocity dispersions and virial masses. The RGH work is for the CfA2. Slices, whose groups show a 60% higher v_{gr} than for their equivalently selected CfA1 groups as a result of differing sample depth and, to some extent, cosmic variance (see RGH for discussion). Also, their link parameters differ from ours. They used a smaller sky link (giving smaller r_h) but larger redshift link, leading to higher v_{gr}'s and net higher M/L's.

When using full three-dimensional information to make sky catalog groups (sky link 0.36 as before, equal now to $D_n \equiv D_0$ normalized to the completeness at that distance), our median Ω's are higher: $\Omega_0 = 0.16$ (both CHDM), 0.32 (CDM1.5), and 0.48 (CDM1). Note that the V_5's necessary to match three-dimensional v_{gr}'s are, except for CDM1.5, higher than our fiducial V_5, as shown in Table 3. For example, raising CHDM's V_5 from the fiducial 350 to 397 km s^{-1} raises $\langle v_{gr} \rangle_{med}$ by $\sim 15\%$, and therefore $\langle M/L \rangle_{med}$ and Ω_0 by $\sim 32\%$, lessening the difference between the observationally inferred and true Ω. The same holds for CDM1. Our CDM1.5 estimate of $\Omega_0 \simeq 0.33$ (for Table 3, $V_5 = 572$ km s^{-1}) agrees well with that of Katz et al.'s (1992) TREESPH hydrodynamic simulation result of $\Omega_0 \simeq 0.31$ on a much smaller sample.

9. GROUP STATISTICS USED AS COSMOLOGICAL DISCRIMINATORS

NKP94 showed that the rms group velocity (the usual velocity dispersion) v_{gr} versus the fraction of galaxies in groups f_{gr}, plotted against changing redshift link V_5, was a promising discriminator between these cosmological models. The reason is that the hot dark matter's infall is delayed, reducing the acceleration given to the cold fraction during its collapse and therefore reducing the small-scale random velocities. This has two effects: v_{gr} is lower for higher Ω_ν, while at the same time, the lower v_{gr} on small scales permits easier grouping in redshift space, and therefore higher f_{gr}. Both effects tend to separate curves in the v_{gr} versus f_{gr} plane. Put another way, the "pressure" provided by CDM's higher small-scale velocities will tend to expand structures on megaparsec (i.e., galaxy group) length scales. In Figures 12*a* and 12*b*; we replot NKP94's Figure 3 for the full 10.384 sr sample and the sky catalogs cut to the CfA1 geometry, respectively, both using our new sky catalogs constructed with the revised procedures described earlier. The statistics here have also been subjected to an additional refinement to correct for the fact that the number of groups versus redshift differs between the observed and simulated data because of large-scale structure and also the repli-

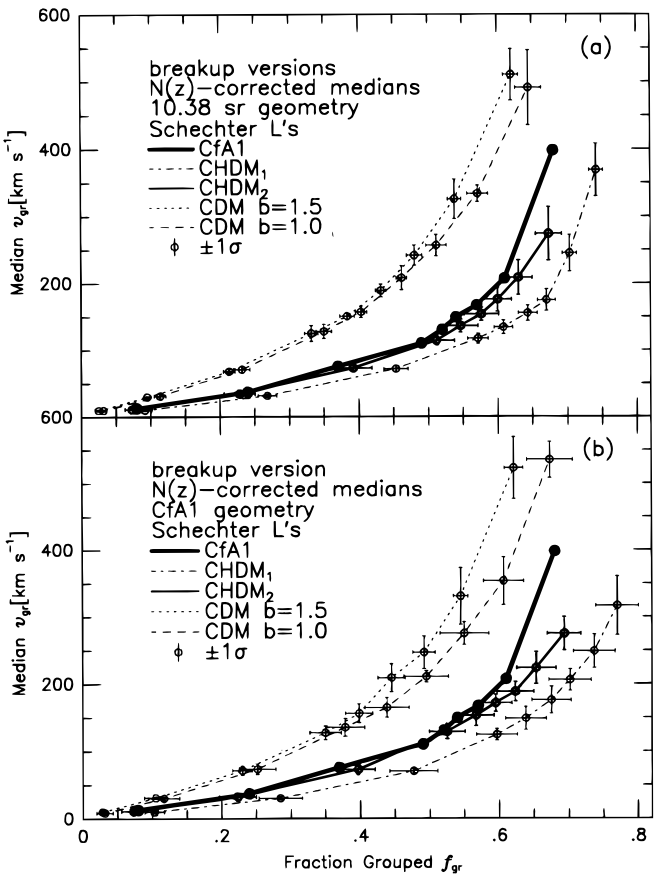

FIG. 12.—Statistic v_{gr} vs. f_{gr} under varying V_5 for our fully corrected case using (*a*) the 10.384 or sky catalogs and (*b*) the 2.66 CfA-like sky catalogs.

cation of periodic boxes. Since in a magnitude-limited catalog more distant groups are brighter and likely to be systematically different in other ways, we binned the groups in 1000 km s^{-1} bins and then drew random samples from the simulation groups such that they reproduced the observed number of groups versus redshift $N(z)$ of CfA1. This was done several times and averaged before taking medians. Since there is a large void beind Virgo, this "$N(z)$ correction" de-weighted the distant, massive, high-v_{gr} simulation groups, and therefore dropped the curves slightly relative to NKP94. Here and throughout this paper, the v_{gr}'s for CfA1 groups are corrected by subtracting in quadrature the published rms velocity measurement errors for the member galaxies from the raw v_{gr}'s. The CDM curves are now closer to that of CfA1 but otherwise the new figures are quite similar. These figures change quantitatively very little and qualitatively not at all when using the Cen-Ostriker or Tully-Fisher luminosity assignments to construct sky catalogs. They also change very little when using the "method 2" or "method 3" breakup methods (at a given v_{gr}, f_{gr} drops by ~ 0.05). However, using the "method 1" scheme raised f_{gr} dramatically, since this assigned nearly equal luminosities to the breakup fragments and therefore kept them in the catalog even after magnitude limiting. The result is that all simulations are nearly degenerate, with f_{gr} far above that for CfA1.

It may be surprising to see that the curve for CDM1.5 differs so little from that of CDM1, since numerous studies, including Figure 3 here, show biased CDM has lower velocities. Our global rms peculiar velocities (i.e., for all galaxies within the box) are indeed much lower for CDM1.5 than those for CDM1: 650 km s^{-1} versus 944 km s^{-1}. Within groups, however, two different effects combine to reduce this difference. First, on small scales ($\simeq 1$ Mpc), CDM1.5 rms peculiar velocities are only 23% lower than for CDM1. This is true both for the full set of box groups, and for the three-dimensional selected groups from the sky catalogs. With the same $V_5 = 600$ km s^{-1} on both CDM simulations, median v_{gr}'s differ by only 9% (189 km s^{-1} for CDM1.5 vs. 207 km s^{-1} for CDM1). This same effect is seen in Moore, Frenk, & White (1993), and our result agrees well with the 8% difference seen between their $b = 1.6$ and $b = 2.0$ CDM median v_{gr}'s. Second, while the overall number of galaxies of the two CDM simulations differ by $\sim 20\%$, when normalized to CfA1 their spatial structures are such that, blurred in redshift space, CDM1.5 actually groups less easily than CDM1.5 at the same V_5, despite its lower velocities. This counters the differing v_{gr}'s and results in the curves being quite close together. Somerville et al. (1997) has reexamined the CfA1 pairwise velocity dispersion, which includes this effect, and also find relatively poor discrimination between CDM1 and CDM1.5.

We now present group analyses of two new 100 Mpc box PM simulations that raise a strong caution to Figure 12. The simulations model a "two-neutrino" (2ν) CHDM model with $\Omega_\nu = 0.2$ shared equally between two neutrino species (Primack et al. 1995). Two such simulations were run in 50 h^{-1} Mpc boxes with 256^3 cold particles and 2 times as many hot particles, one at 512^3 and one at 800^3 resolution with identical parameters and initial conditions. Halo mass measures were calculated from densities in a grid of 10 radii from halo center, a big improvement over the one-cell and three-cell mass measures used in the 512^3 simulations discussed above. the 512^3 2ν simulation was broken up by the "adopted method" already described. The 800^3 simulation was broken up ("$z = 0$ breakup") in a way similar to the 512^3 adopted method, but based on a new hydrodynamic $\Omega = 1$ CDM simulation of Evrard—which improves on ESD by simulating a more typical 20 Mpc^3 region rather than their small cluster environment—and evolving all the way to $z = 0$ (but still without star formation feedback). Most Evrard halos above a logarithmic mass log $M_{170} = 12.1$ (defined within a radius r_{170} enclosing an average overdensity of 170) contain multiple "globs" (galaxy-like objects; see ESD), and we assigned a sliding probability (linear in log space) $P = 0 \rightarrow 1$ for breakup corresponding to log M_{170} from 11.4 to 12.7. Breakup fragments this time were placed randomly, without regard for enforcing a uniform spatial resolution, within a radius r_{170} of the overmerger and with Schechter distributed fragment masses. Fragment velocities were assigned as in the "adopted method." Because M_{bu} is measured inside a much lower overdensity radius—r_{170} rather than the r_{1360} extrapolated from the $z = 1$ ESD results—and with better spatial and force resolution (which effectively deepens potential wells), it is effectively somewhat lower than the M_{bu} of the adopted method above (even though numerically higher), and results in a much higher number of overmergers and breakup fragments. Put another way, our poorer resolution at 512^3 reduced the amount of mass inside the extrapolated, very deep overdensity of 1360, strongly reducing the number of overmerger candidates. Applying the $z = 0$ breakup to the 512^3 2ν simulation shows that the rise in the number of overmergers is due about equally to the higher resolution and to the $z = 0$ breakup prescription. While fully 89% of the resulting sky catalog galaxies are either central overmerger fragments (57%) or secondary fragments (32%), the central fragments retain phase space coordinates quite similar to their parent overmergers, so that only 32% of the sky catalog galaxies are highly sensitive to the assumptions of our breakup. Nevertheless, this leads to major changes in the observed group properties. Figure 13 compares breakup and no breakup versions of the 2ν sky catalogs cut to CfA1 geometry. At 512^3 resolution, 2ν results are reasonably robust against the adopted breakup method, just as with CDM and CHDM. The expression f_{gr} rises and v_{gr} drops slightly, both by about 1 σ for all grouping linkages. Since the appropriate comparison is to the unmerged CfA1 curve, which is also shifted down and to the right, the net change is quite small. But at 800^3, with the improved $z = 0$ breakup method, v_{gr} drops by $\sim 25\%$–40% and f_{gr} rises substantially by ~ 0.1–0.2, so that v_{gr} versus f_{gr} shifts strongly to the right and below the CfA1 curves. While, if taken at face value a similar shift of our CDM and CHDM curves would imply a favored $\Omega_\nu < 0.2$, as well as a slightly higher optimum V_5 for identifying conventional groups, the main point is that group statistics on these pure dissipationless catalogs are clearly not robust under this breakup. With its higher resolution and better determined M_{bu} and mass measures, this new breakup is better motivated than the ESD-inspired "adopted method" used earlier and in NKP94, so this point must be taken seriously.

It is uncertain whether other hydrodynamic simulations will confirm this significant overmerging. For example, a preliminary visual inspection of a recent TREESPH CDM simulation by Hernquist, which included stellar feedback (importantly, though, not magnitude limited, which would

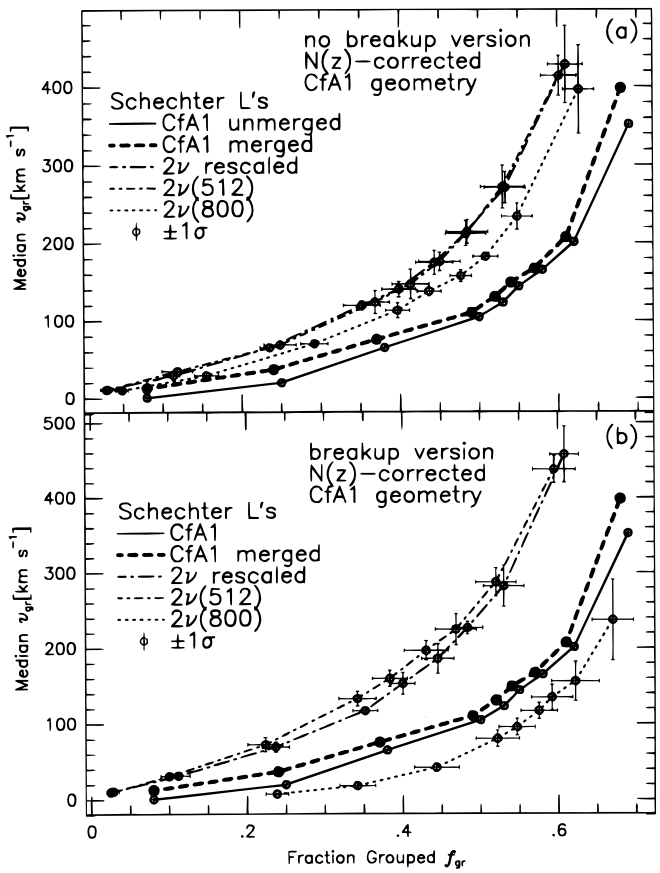

FIG. 13.—Comparison of the two-neutrino model at 512^3 and 800^3 resolution for the (*a*) no breakup and (*b*) breakup cases, together with the merged and unmerged CfA1. "2ν rescaled" is the 800^3 simulation data rebinned at 512^3 resolution and analyzed the same as the other 512^3 simulations. The strong shift of the 2ν(800) curve shows that these statistics are sensitive to the presence of overmerging.

have strongly favored massive objects), did not show obvious overmerging outside a central cluster. On the other hand, our Evrard-inspired new log $M_{bu} = 12.1$ inside overdensity 170 is equivalent to the Milky Way mass out to $r_{170} \sim 310$ kpc (Kochanek 1996), which is about the gravitational halfway point to Andromeda, and so does not seem unreasonably low. Indeed, assuming Andromeda is 2 times as massive as Kochanek's Galaxy, our new beakup applied to the Galaxy + Andromeda systems correctly predicts the three visible galaxies that would actually be seen in the CfA1 at 700 km s^{-1} distance, along with the 3–4 additional companion fragments that would be just below visibility. It is possible that, in general, sufficient energy input from an initial burst of star formation may suppress the collapse of enough of the remaining baryons that they too may "overmerge" along with the dark matter, leaving fewer satellite galaxies than we have inferred here. However, energy input from photoionization has little effect in preventing baryonic condensation down to the 10^{10} $M_\odot$ level (Weinberg, Hernquist, & Katz 1997; Quinn, Katz, & Efstathiou 1996). These same studies show that photoionization's apparent ability in earlier studies to suppress even relatively massive galaxies is an artifact that disappears at higher resolution. Instead, star formation feedback must be delivered as kinetic energy to prevent condensation, and it is unclear whether improved simulations will see this. For now, we conclude that reliable cosmological tests using group analysis, and perhaps most other galaxy-based statistics as well, must await higher resolution simulations that include more of the relevant physics of star formation.

10. CONCLUSIONS

Our first and most secure conclusion is that, within the models we have studied, it is quite natural to find $\Omega_0 \sim 0.1$ from group mass to light ratios, even when the true Ω_0 is 1. Three factors combine in the same direction to severely bias the M/L method on the low side. First, galaxies within a group occupy only the central core of much larger DM concentrations. The total mass bound to the group at $2r_h$ is a factor of 3 higher than the DM within r_h. Second, the appropriate virial mass to calculate is that caused by the individual cold DM particles, not the galaxies, whose velocity bias contributes another factor of ~ 2. Finally, the virial theorem implicitly assumes spherical symmetry, and our groups are actually fairly elongated. Counting mass within these elongated boundaries will add perhaps another 30% to the true mass, giving a net correction to M/L of nearly an order of magnitude. Hot DM that is unclustered will further bias M/L to the low side. This low bias to inferred Ω seems quite secure, even at higher resolution. The new $z = 0$ breakup of our 800^3 2ν simulation, when compared to the 512^3 broken up by the "adopted method," shows v_{gr} lower by $\sim 40\%$ and r_h lower by $\sim 65\%$, and giving lower virial M/L and Ω. The major reason for the bias is likely to be the strong concentration of galaxies relative to the dark matter, and breaking up overmergers only increases this concentration.

Our second conclusion is that these group statistics, especially v_{gr} versus f_{gr}, show strong sensitivity to the fraction of hot dark matter in CDM, while at the same time showing much less sensitivity to the normalization within CDM. The statistics appear robust to several reasonable methods of illuminating the halos, but they are apparently quite sensitive to the relatively poor force and spatial resolution used here, as well as to how overmergers are broken up.

Our third conclusion is that group statistics appear to imply an Ω_ν less than 0.3, since breakup almost certainly raises f_{gr} while having less effect on v_{gr}, and even with no breakup the v_{gr} versus f_{gr} statistic for $\Omega_\nu = 0.3$ CHDM favors a slightly lower Ω_ν. With less confidence, the 2ν results suggest $\Omega_\nu < \sim 0.2$.

Finally, since higher Ω_ν clearly lowers small-scale velocities and raises small-scale correlations, we believe f_{gr} versus v_{gr} applied in redshift space will, when the sites of galaxy formation can be reliably determined in large-scale simulations, ultimately prove to be a powerful discriminator between these cosmologies.

It is a pleasure to thank Gus Evrard for supplying key results, and to acknowledge insightful and sometimes spirited discussions with Neal Katz and David Weinberg. We also thank Jerry Ostriker for suggesting the Cen-Ostriker work as a way to relate mass to luminosity and an anonymous referee for helpful suggestions. R. N. gratefully acknowledges a NASA grant administered by the American Astronomical Society and a continuing grant of computer resources by UCO/Lick Observatory. A. K. and J. R. P. acknowledge support from NSF and NASA grants. The simulations were run on the Convex C-3880 at the NCSA Champaign-Urbana, IL.

REFERENCES

Baugh, C. M., & Efstathiou, G. 1993, MNRAS, 265, 145
Bennett, C. L., et al. 1996, ApJ, 464, L1
Bird, C. M. 1994, AJ, 107, 1637
Borgani, S., et al. 1997, New Astron., 1, 321
Brodbeck, D., Hellinger, D., Nolthenius, R., Primack, J. R., & Klypin, A. A. 1997, ApJ, submitted (BHNPK)
Bryan, G. L., Klypin, A. A., Loken, C., Norman, M. L., & Burns, J. O. 1994, ApJ, 437, L5
Caldwell, D. O. 1995, Nucl. Phys. B., S43, 126
Carlberg, R. G. 1994, ApJ, 433, 468
Carlberg, R. G., & Couchman, H. M. P. 1989, ApJ, 340, 47
Cen, R., & Ostriker, J. P. 1993, ApJ, 417, 387 (CO93)
Crone, M. M., Evrard, A. E., & Richstone, D. O. 1994, ApJ, 434, 402
Davé, R., Hellinger, D., Primack, J. R., Nolthenius, R., & Klypin, A. A. 1997, MNRAS, in press
Davis, M., Huchra, J., Latham, D. W., & Tonry, J. 1982, ApJ, 253, 423
de Lapparent, V., Geller, M. J., & Huchra, J. P. 1986, ApJ, 332, 44
Efstathiou, G., Ellis, R., & Peterson, B. A. 1988, MNRAS, 232, 431
Evrard, A., Summers, F., & Davis, M. 1994, ApJ, 422, 11 (ESD)
Fahlman, G., Kaiser, N., Squires, G., & Woods, D. 1994, ApJ, 437, 56
Feldman, H., Kaiser, N., & Peacock, J. A. 1994, ApJ, 426, 23
Fisher, K. B., et al. 1993, ApJ, 402, 42
Fouque, P., Bottinelli, L., Gougenheim, L., & Paturel, G. 1990, ApJ, 349, 1
Frederic, J. J. 1995a, ApJS, 97, 259
———. 1995b, ApJS, 97, 275
Frenk, C. S., Evrard, A. E., White, S. D. M., & Summers, F. J. 1996, ApJ, 412, 460
Gelb, J. 1992, Ph.D thesis, MIT
Geller, M. J., & Huchra, J. P. 1983, ApJS, 52, 61
Ghigna, S., Borgani, S., Bonometto, S. A., Guzzo, L., Klypin, A. A., Primack, J. R., Giovanelli, R., & Haynes, M. 1994, ApJ, 437, L71
Ghigna, S., et al. 1996, ApJ, 469, 40
Giavalisco, M., Steidel, C. C., & Szalay, A. S. 1994, ApJ, 425, L5
Hockney, R. W., & Eastwood, J. W. 1981, Computer Simulations Using Particles (New York: McGraw-Hill)
Holtzman, J. A., & Primack, J. R. 1993, ApJ, 405, 428
Hu, E. M., & McMahon, R. G. 1996, Nature, 382, 231
Huchra, J. P., & Geller, M. J. 1982, ApJ, 257, 423 (HG82)
Katz, N., Hernquist, L., & Weinberg, D. 1992, ApJ, 399, L109
Katz, N., & White, S. D. M. 1993, ApJ, 412, 455
Kirschner, R., Oemler, A., & Schechter, P. 1979, AJ, 84, 951
Klypin, A. A., Borgani, S., Holtzman, J., & Primack, J. R. 1995, ApJ, 444, 1
Klypin, A. A., Holtzman, J. A., Primack, J. R., & Regős, E. 1993, ApJ, 416, 1 (KHPR)
Klypin, A. A., Nolthenius, R., & Primack, J. R. 1997, ApJ, 474, 533 (KNP)
Klypin, A. A., & Rhee, G. 1994, ApJ, 428, 399
Kochanek, C. S. 1996, ApJ, 457, 228
Kolatt, T., & Dekel, A. 1997, ApJ, 479, 592
Mamon, G. 1994, in Clusters of Galaxies, Proc. XIVth Moriond Astrophysics Meeting, ed. F. Durret, A. Mazure, S. D. M. White, & J. Tran Thanh Van (Gif-sur-Yvette: Editions Frontieres), 291
Mo, H. J., & Fukugita, M. 1996, ApJ, 467, L9
Moore, B., Frenk, C. S., & White, S. D. M. 1993, MNRAS, 261, 827
Navarro, J., Frenk, C. S., & White, S. D. M. 1996, ApJ, 563
Nolthenius, R. 1993, ApJS, 85, 1 (N93)
Nolthenius, R., Klypin, A. A., & Primack, J. R. 1994, ApJ, 422, L45 (NKP94)
Nolthenius, R., & White, S. D. M. 1987, MNRAS, 225, 505, (NW87)
Plionis, M., Borgani, S., Moscardini, L., & Coles, P. 1995, ApJ, 441, L57
Pogosyan, D. Y., & Starobinsky, A. A. 1995, ApJ, 447, 465
Primack, J. R., Holtzman, J., Klypin, A., & Caldwell, D. O. 1995, ApJ, 447, 465
Quinn, T., Katz, N., & Efstathiou, G. 1996, MNRAS, 278, L49
Ramella, M., Geller, M. J., & Huchra, J. P. 1989, ApJ, 344, 57 (RGH)
Schechter, P. 1976, ApJ, 203, 297
Schlegel, D., Davis, M., Summers, F., & Holtzman, J. A. 1994, ApJ, 427, 527
Seljak, U., & Bertschinger, E. 1994, ApJ, 427, 523
Somerville, R. S., Primack, J. R., & Nolthenius, R. 1997, ApJ, 479, 606
Steidel, C. C., et al. 1996, ApJ, 462, L17
Storrie-Lombardi, L. J., McMahon, R. G., Irwin, M. J., & Hazard, C. 1995, ApJ, 427, L13
Summers, F. J., Davis, M., & Evrard, A. E. 1995, ApJ, 454, 1
Tully, R. B. 1987, ApJ, 321, 280
Weinberg, D., Hernquist, L., & Katz, N. 1997, 477, 8